Flow patterns in partially vegetated channels :

Combining physical experiments and numerical modelling

Yunze Zhu

in partial fulfilment of the requirements for the degree of Master of science in Hydraulic Engineering at Delft University of Technology

August, 2017, Delft

To be defended publicly on Wednesday August 30th, 2017

Graduation Committee:

Prof.dr.ir Aarninkhof, S.G.J. (chair)	Delft University of Technology
Prof.dr.ir. Stive, M.J.F.	Delft University of Technology
Prof.dr.ir. Uijttewaal, W.S.J.	Delft University of Technology
Dr. Quinghua, Y.E.	Deltares
Truong Hong, S.	Delft University of Technology

Acknowledgments

This report is the final requirement for completion of the MSc programme in Hydraulic engineering under department of coastal engineering in Delft University of Technology. This research mainly focuses on the influence of physical parameters (e.g. Bed roughness and drag coefficient) and environental settings on flow characteristics in a partially vegetated compound channel. During this thesis project, I have received help from people in TU Delft and Deltares, without which I would not be able to finish this project.

Firstly, I would like to thank my supervisors Truong Hong Son and Dr. Qinghua Ye for sharing their expertise and time. Their guidance has always been very helpful in perspectives of flume experiments and model setup. Secondly, I would like to thank Prof. Uijttewaal, who has supported me by providing expertise of turbulence. Thirdly, I would like to thank Prof. Aarninkhof, who is the chair of my project group, for sharing his time and giving useful suggestions. I would like to express my thanks to Prof. Stive for giving me the opportunity to start this project and giving helpful suggestions.

Finally, I would like to thank my family and friends who support me all the time and cheer me up when I met difficulties.

Yunze Zhu

Summary

As coastal wetland ecosystems, thriving at the interface between land and water, mangroves can benefit us in lots of ways: providing food and timber, purifying water and sequestrating carbon, protecting coastal area through wave attenuation and coastal stabilization. Regarding the protection of coastal area, mangroves damp the flow in short term and mitigate coastal erosion in long term.

In mangrove forests, the capability of mangroves to capture sediments leads to accumulation of sediments within the mangrove forests. Hence, the elevation of the floodplain, where the mangroves grow, is usually higher than the main river bed. The slope connecting the main river channel and floodplain has been found with different angle. The topography of the mangrove area is influenced by both sediment dynamics and hydrodynamics. The physical processes behind this is still not fully understood. This study aims to study the hydrodynamics in a partially vegetated compound channel by using the 2DH RANS model in Delft3D and to verify to what extend the flow characteristics can be reproduced. The reference numerical model is set up to mimic the flume experiments so that the model can be calibrated. The influence of different physical and environmental parameters on flow characteristics is studied. Also, the limitation of Delft3D in simulating the flow in a partially vegetated compound channel has been found.

Combining the flume measurements and calibration of the model suggests a manning coefficient of 0.0021 $m^{1/3}/s$. This value is around an order of magnitude smaller than the bed roughness in a large scale flow (prototype). This implies that the bed roughness input should be smaller in a small scale flow than that in a large-scale flow. The drag coefficient is 1 for single cylinders and in this study a value of 0.8 is recommended after calibration of the model. This means the drag coefficient should not deviate too much from 1. An uniform horizontal eddy viscosity value of $10^{-4} m^2/s$ is suggested according to calibration of the model. In large scale flow this value is still applicable according to the tests and reasonable results can be seen. It is recommended to keep this value as small as possible since the coherent structures are damped out as background eddy viscosity increases.

Some limitation of the RANS model in Delft3D-Flow has been found when it is applied to a partially vegetated compound channel. Firstly, a space varying background horizontal eddy viscosity (e.g. Triangular distribution) in RANS model may not be sufficient to model the shear layer vortices since in reality the horizontal eddy viscosity should be both time and space varying. This implies that the model concept of background horizontal eddy viscosity is not very practical. Secondly, after analyzing the model results, it is found that the model is not very accurate in predicting the momentum transport in the shear mixing layer and the momentum exchange is too much around the edge of vegetation patch. This leads to an

underestimation of flow velocity in the shear mixing layer and an overestimation of eddy penetration into the vegetation patch. The possible reason is that the vegetation model only takes into account the overall effects of vegetative drag force instead of considering the effects of each single stem. The flow behavior in the main channel is not influence by the shear mixing layer and in the model it can be well reproduced. Regarding the predictive ability of the model, it is believed that the model can give reasonable results for lateral velocity profile and large scale turbulence. It is still applicable to cases when the requirement of accuracy is not very high (e.g. studying the influence of vegetation on flow characteristics).

Under the assumption that the model is able to capture the changes of flow characteristics when physical parameters or environmental settings are changed, a further research focuses on the influence of environmental settings on flow characteristics. Regarding the influence of vegetation on flow, it is found that the vegetation patch strengthen the momentum exchange in the shear mixing layer. The slope angle is also influential in case with dense vegetation on the floodplain. A slope angle around 1/10, which is the most typical slope angle in Mekong estuarine system, leads to the largest amount of momentum transport into the vegetation patch. Also, with a slope angle of 1/10 the strongest eddy structure is observed. This implies that a 1/10 slope could be a result of natural selection.

Contents

Chapter 1

Introduction

As coastal wetland ecosystems, thriving at the interface between land and water, mangroves can benefit us in lots of ways: providing food and timber, purifying water and sequestrating carbon, protecting coastal area through wave attenuation and coastal stabilization. Regarding the protection of coastal area, mangroves damp the waves and flow in short term and mitigate coastal erosion in long term. It is reported that mangroves weakened the impact of the 2004 Indian Ocean tsunami by reducing damage and saving lives in coastal area (Danielsen et al., 2005).

However, the total area of mangrove forests worldwide is experiencing a rapid decline of 1 to 2% per year (Duke et al., 2007). This is caused by combined effects of sea-level rise and human activities. Doody(2004) introduced a term ‘‘squeeze’’ to describe this phenomenon. The effect of sea-level rise tends to make mangrove forests retreat landward while the human activities such as urbanization, agriculture, and aquaculture prevents the mangroves from retreating. Consequently, the mangrove forests are pushed into a narrower fringe. The effect of human activities usually happens in a shorter period with a larger impact than the effect of sea-level rise.

Son (2017) believed that there exist a minimum width of mangrove forests for the survival of the ecosystem and for the case in Mekong estuarine system(MES) the minimum width is around 80 m. This phenomenon can be explained from the perspectives of energy and cyclic evolution of vegetation. Regarding the research by Son (2017), a numerical model (Delft3D) is used to study the relation between the minimum width of mangroves and the maximum penetration length of flow. The numerical model in his study still needs to be calibrated and validated. This study aims to understand the physical processes and the limitation of Delft3D by calibrating the numerical model and analyzing the model output. A 2DH (two-dimensiontal horizontal) RANS model is used in this study. Through this study, on one hand an understanding of the physical processes in a partially-vegetated compound channel will be obtained and on the other the limitation of Delft3D in simulating the flow characteristics in a partially vegetated channel will be realized.

1.1 A brief overview of mangrove characteristics

The definition of mangroves

Mangroves are tidal forest ecosystems that are found in low-energy saline or brackish environments, such as the intertidal area of estuaries and marine shoreline. The composition of vegetation in mangroves includes shrubs and trees, which can reach up to 30-40 m height under ideal conditions (Tomlinson, 1986). Mangrove forests are able to survive in harsh environment such as high salinity, high temperature, extreme tides, high sedimentation and muddy anaerobic soils (Giri et al., 2011).

Global and regional context of mangroves

Mangroves thrive worldwide in tropics and sub-tropics because of their frost intolerance[Tomlinson, 1986], mainly between 30° N latitude and 40° S latitude (Figure 1.1) with largest densities between 5° N and 5° S latitude[Spalding et al., 2010; Giri et al., 2011]. The total area of mangroves was estimated at 137,760 km^2 in 118 countries by the year 2000 (Giri et al., 2011). Six tropical regions of mangroves globally can be distinguished based on the continental borders : Western America, Eastern America, Western Africa, Eastern Africa, Indo-Malaysia and Australia (Duke, 1992). Approximately 75% of mangroves globally are concentrated in only 15 countries and the largest portion is found in Asia (42%)(Giri et al., 2011).

Figure 1.1 – Global mangrove distribution in 2000. From: Giri et al. [2011].

The physical experiment in this study is based on the case in Tieu estuary, Vietnam. Although the physical experiments are un-scaled due to restrictions in facilities, the most important features are captured such as a 1/10 slope and characteristics of mangroves. Mangroves in Vietnam belong to the Indo-Malaysian class, which features the greatest biodiversity in the world with 51 species out of around 70 species occurring worldwide (Duke, 1992; Alongi, 2002).

Lugo and Snedaker (1974) divided mangroves into six classes based on a functional classification of mangrove forests, namely: fringing, riverine, over wash, basin, scrub and hammock. This classification was rearranged and simplified into three main

classes by Cintron and Novelli (1984) based on landforms: fringing, riverine and basin mangrove. Woodroffe (1992) proposed a classification based on physical processes and differentiate mangrove habitats between tide-dominated, river-dominated and interior mangroves.

Fringing (tide-dominated) mangroves usually thrive at low-gradient intertidal areas of sheltered coastline. They are exposed to strong bi-directional tidal flow and possibly waves in case they face the open sea (coastal mangrove). Riverine mangroves (river-dominated) mangroves situate along the river bank, such as deltas of large rivers. They are usually exposed to uni-directional water flows during flood tides. Basin(Interior) mangroves mostly dominate in inland depressions so that they are least exposed to waves and tidal motions (Lugo and Snedaker, 1974; Woodroffe, 1992; Ewel et al., 1998; Mazda et al., 2007).

It should be noticed that the above-mentioned classification only take into account the effect of tidal action and river flow while the influence of waves is neglected. This makes it difficult to fully understand the differences of bio-physical interaction in coastal and estuarine mangroves. This is especially the case in Mekong estuarine systems(MES) where the tides and waves both affect the region. Thus Son (2017) proposed a new classification, which includes three main categories: Fringing Coastal mangrove (FC), Fringing Estuarine mangrove (FE) and Interior mangrove (I). FC are the mangrove forests located at coastal regions and are mainly exposed to waves and tide. FE thrives at estuarine regions, mainly influenced by tidal action and geometric features of the river. The combined effects of tidal flow, river flow and lateral flow are important for these two types of mangrove forests. Interior mangroves(I) are protected and least exposed to waves and tides. In this paper, only FE will be studied.

The succession in mangroves

The environment in mangrove forests is stressful to most plants due to the high salinity and frequent inundation. However, mangrove species can tolerate this environment and assemble into forests. Thus, the succession in mangroves is related to the environmental tolerances of the species, which often leads to distinct distribution of mangrove species in different locations.

The succession form of mangrove forests in the MES is composed of the mangrove species that dominate land edges and those that dominate water edges. The latter usually experience the following main stages (Phan and Hoang, 1993). The pioneer stage describes the stage when mangrove species such as *Sonneratia and Avicennia* establish themselves on frequently inundated tidal flats. These species can tolerate high salinity and frequent flooding. They both have pneumatophores roots, which support them in the substrate. During the transitional stage, pneumatophores systems of *Sonneratia and Avicennia* can trap sediment and soil, which leads to the elevation of mudeflats. Then tidal water brings the seedlings of other land edge species such as *Nypa fruticans, Cryptocoryne ciliata* and *Acanthus ilicifolius* to the flats and they are trapped by the pneumatophores system. As the mudflats are continuously

elevated by sediment deposition, the land might only be flooded during high tide, which leads to the final stage . The final stage features species communities with great bio-diversity. Land edge mangrove species such as *Derris trifoliate, Wedellia biflora, Acanthus, ilicifolius* are able to survive.

Estuarine mangroves, on the other hand, usually consist of a mixed type of species that can tolerate a wide range of salinities. These species include *Sonneratia Alba, Avicennia alba* , *Acanthus ilicifolius, Nypa fruticans* and *Cryptocoryne ciliata* etc.

In the schimatised model, the characteristics of vegetion must be defined in detail. In the schematized model of this study, the estuarine mangrove forests only consist of *Sonneratia*, which is known by its pneumatophores.

1.2 Interaction between river channel and mangroves

As mentioned in Chapter 1.1.2, this study only focuses on fringing estuarine mangroves, which is mainly influenced by tidal action and river flow. The inundation of mangrove forests is caused by combined effects of overbank(sheet) flow and creek flow. Creek flow is usually ebb dominated and the ebbing mainly happens through creek flow (Aucan and Ridd, 2000). Horstman (2014) concluded that for the highly elevated mangroves, creek flow dominate when water levels remain below the high-density vegetation layer and overbank flow prevails when this threshold is exceeded. The distinction of creek flow and sheet flow is important since the flow routing can directly influence the supply of sediment and nutrients into mangroves. However, creek flow is neglected in this study since hardly any creek is observed in MES. The flow routing behaves differently when there is no creek. Kobashi and Mazda(2005) observed that in a smoothly sloping mangrove fringe without creeks, flow is parallel to the river at the interface of river and vegetation and it gradually turns perpendicular to the river further inside the forest.

The presence of mangroves alters the stream flow and create a mean velocity difference between flow in mangrove and main river channel. This leads to the formation of a shear mixing layer where transportation of mass and momentum occurs (see figure 1.2). The penetration length of the shear layer is important to the sustainability of mangrove forests since space is needed to absorb the flow energy. If the width of the forest is larger than the penetration length, flow is dampened and the environment is favorable for sedimentation and propagules (Son,2017). This study mainly focuses on the simulations of flow patterns in and near mangrove forests with Delft3D.

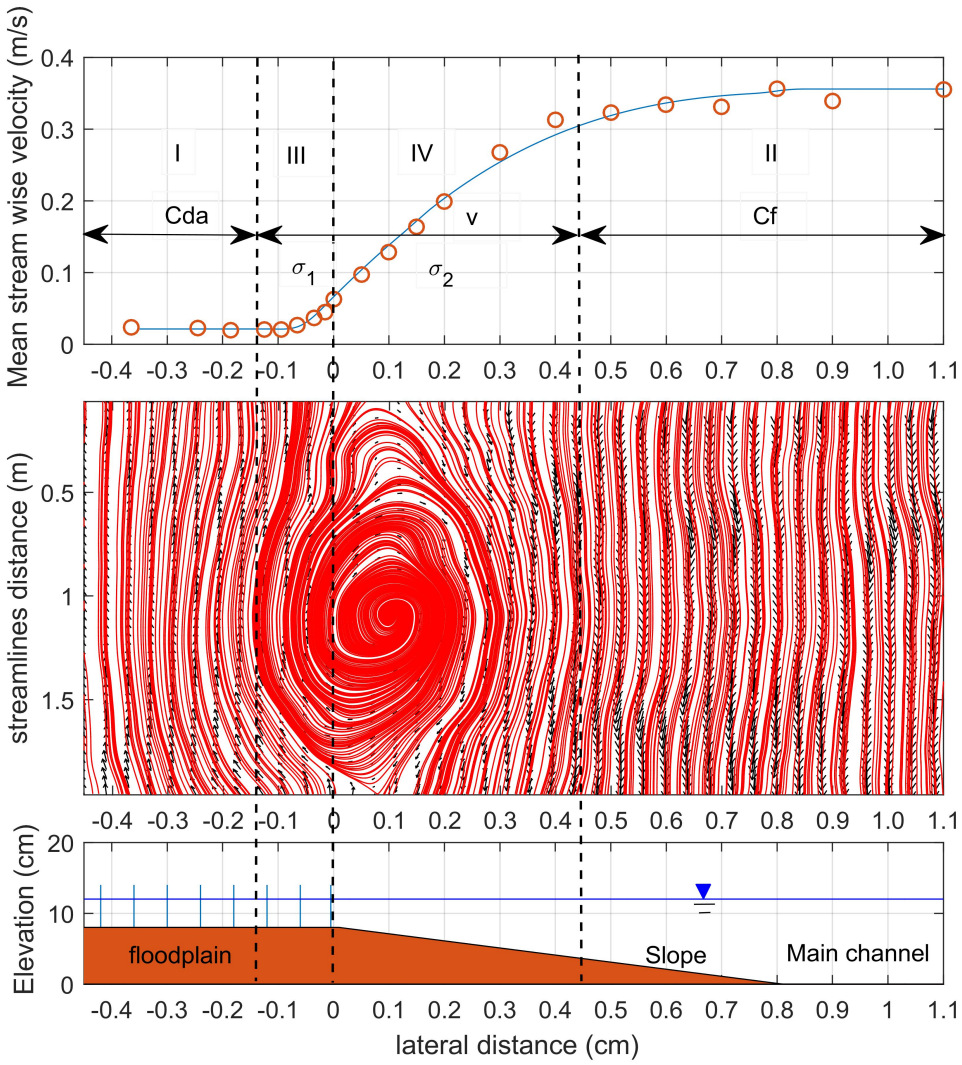

Figure 1.2 : The upper pannel shows the lateral velocity profile in a partially vegetated compound channel. The middle pannel shows the large scale horizontal coherent structures in the shear mixing layer. The lower pannel shows the topography of the channel.

The flow in an open channel adjacent to a patch of emergent vegetation shows four different flow regions (Buckman, 2013), as can be seen in Figure 1.2.

(1) The first region is the area in the vegetation patch and far from the interface of vegetation and main channel. The flow velocity in this region is uniform and influenced by the aggregated vegetative drag and turbulent stress.

(2) The second region is the area in the main channel far from the vegetation patch and other boundaries. The flow in this area is a typical open channel flow and the depth-averaged velocity is uniform in this area. The flow velocity in this region is dominated by the bed friction and wall roughness at the closed boundaries.

(3) and (4) The third and fourth regions are inner shear layer and outer shear layer respectively, which are located around the interface of the main channel and the

vegetation patch. The flow in this transitional zone features rapidly decreasing depth-averaged velocity towards the vegetation patch. This leads to the formation of the mixing shear layer where momentum and mass exchanges happen. The flow velocity in this region is dominated by the shear-layer vortices and momentum exchange.

1.3 Statement of the problem

There are already some studies providing insight into flow patterns within vegetation by combining field, flume and modeling experiments (Temmerman et al., 2005b; Bouma et al., 2007). However, these studies mainly focused on salt marshes rather than mangroves. The large difference between mangroves and salt marshes such as the size and densities of the vegetation structures makes the outcomes from studies of salt marshes can not be used for mangroves. Horstman (2014) combined field data and numerical modeling to study the implications of the tidal flow routing for the depositional patterns. However, the focus is more on the depositional patterns. Son (2017) utilized numerical Model (Delft3D) to study the relation between the minimum width of mangroves for survival and the maximum penetration length of flow. However, the physical processes in such a flow field and the limitation of Delft3D still needs to be studied.

In mangrove forests, the capability of mangroves to capture sediments leads to accumulation of sediments within the mangrove forests. Hence, the elevation of the floodplain, where the mangroves grow, is usually higher than the main river bed. In Mekong estuarine systems, the slope which connects main river channel and floodplain is around 1/10 (Son, 2017). However, a milder slope was measured in Trang province,Thailand with an angle between 1/1000 to 15/1000 (Horstman,2014). The topography of the mangrove area is influenced by both sediment dynamics and hydrodynamics. The physical processes behind this is still not fully understood and very few literature studied the effects of geometrical settings on flow characteristics. In this study, only the hydrodynamics in a partially vegetated channel is studied due to a lack of data to calibrate the model with sediments.

In order to study the flow pattern at the interface of mangroves and main channel, three ways can be adopted: field observations, physical experiments and numerical modeling. Numerical model functions as a tool to study the hydrodynamics around mangroves at a higher spatial and temporal resolution and scale (Horstman,2014). It improves our understanding of the bio-physical interaction. However, calibration of the numerical model is required to improve the accuracy. During the calibration of the model, the influence of different physical parameters (e.g. Bed roughness and drag coefficient) on flow characteristics will be studied.

Usually field observations are the first choice to calibrate the model. However, only very limited field data about flow routing within mangroves are available due to poor accessibility and harsh conditions (Horstman,2014). So far the flow routing through the mangroves has only been observed implicitly by measuring water level and velocities within creeks (Aucan and Ridd, 2000). Hence physical experiments are

more feasible in order to calibrate the model.
Through this study, on one hand an understanding of the physical processes in a partially-vegetated compound channel will be obtained and on the other the limitation of Delft3D in simulating the flow characteristics in a partially vegetated channel will be realized.

1.4 Research objectives

The research objectives in this study are made of two steps. The first step is to understand the physical processes by calibrating the numerical model and exploring the influence of geometrical settings on flow characteristics. Special attention is paid into the large scale horizontal coherent structures and momentum exchange at the vegetation-flow interface. The second step is to understand the limitation of Delft3D in simulating the flow characteristics in a partially vegetated channel. Based on these research objectives, research objectives can be understood as solving the two research questions below.

1. How do bed roughness, drag coefficient and horizontal eddy viscosity influence the flow characteristics in a partially vegetated compound channel?

2. How do geometrical settings (bank flow with different slope angle and channel flow) influence the momentum transport at the flow-vegetation interface ?

1.5 Approach

In order to solve the research questions a combination of physical experiments and numerical model is adopted. The physical experiments were conducted by Son (2017) and the most representative results will be used in this study. The detail of the experiments will be presented in next chapter.
The approaches consist of two steps in order to reach the research objectives. Firstly, the numerical model will be set up in accordance with the flume experiments. A series of sensitivity tests will be conducted in order to achieve best agreement between results from flume experiments and numerical model. The physcial processes in such a partially vegetated channel is understood by exploring the influence of geometrical settings on flow characteristics. The calibration of the model will base on the lateral depth averaged velocity profile and the eddy structures. Secondly, the horizontal background eddy viscosity is manually set according to experimental results and different formulas in order to understand the limitation of Delft3D in simulating the flow characteristics in a partially vegetated compound channel.

1.6 Thesis outline

The thesis consists of 4 chapters: introduction, theoretical background, Combining physical experiments and numerical modeling, synthesis. Chapter 1 introduces the context of the project. Chapter 2 summarizes the necessary theoretical background. Chapter 3 is the main chapter, which includes a summary of the flume experiments, the model set up and calibration of the model, the sensitivity tests and the analysis of model output. Chapter 4 draws the conclusion of the thesis and gives recommendations for future research.

Chapter 2

Theoretical background

The flow behavior in a partially vegetated compound channel is highly complex because of the combined effects of bed roughness, drag effects of vegetation, shear mixing layer at the edge of vegetation patch. This leads to lots of research into the turbulent behavior in field and laboratory. Section 1.2 already gives a brief introduction to flow characteristics in different flow regions. This chapter focuses on more detailed theories in perspectives of both physics and numerical model. There are five sections in this chapter. Section 2.1 and 2.2 introduce the physics of the drag effects and vegetation-induced turbulence. Section 2.3 introduce the implementation of the vegetation model in Delft3D . Section 2.4 describes the effects of wall roughness and its implementation in Delft3D. Section 2.5 consists of three parts. The first part explai the concept of eddy viscosity. The second part introduce the horizontal Reynolds stress and momentum transport. The third part explains the detail of the sub-grid scale eddy viscosity model in Delft3D and the reason why the HLES model is not used in this study.

2.1 Drag effects of emergent vegetation

When flow encounters an obstruction, such as a stem, it will be deflected around the obstruction. The flow decelerates as it approaches the obstruction and accelerates as it leaves the obstruction. This leads to a pressure difference between the upstream and downstream of the obstruction and increases the drag force on the obstruction (Buckman, 2013). The drag force follows:

$$F_D = \frac{1}{2}\rho C_D A U^2 \tag{2.1}$$

Wherein C_D is the drag coefficients; A is the obstructed area and U is the mean stream-wise velocity. The drag coefficients C_D is equal to 1 when a single cylinder is considered. When a large uniform patch of vegetation is the obstruction, the area term A is modified so that it takes into account the combined effects of multiple stems (Siniscalchi, F. et al., 2012). In case of a uniform patch of vegetation with same size of stems, the area term is given by a frontal area per volume，

$$a = \frac{NA_i}{(W * L)_{patch} * h_{veg}} \tag{2.2}$$

Wherein N is the number of stems; A_i is the frontal area of one stem; $(W * L)_{patch}$ is the area of the patch and h_{veg} is the wet height of the stem. The density of the vegetation patch can be defined as,

$$\rho_{veg} = \frac{\pi}{4} ad \tag{2.3}$$

In which d is the diameter of the stem. The porosity of the vegetation patch can then be written as $n = (1 - \rho_{veg})$. Spatially-averaged Navier-Stokes continuity (3.4) and momentum (3.5) equations can be used to describe the flow through a patch of vegetation (Nepf, Heidi, 2012). The stream-wise direction is denoted as y and $u(y)$,

$$\frac{\partial n < \bar{u} >}{\partial y} = 0 ; \tag{2.4}$$

$$\frac{Dn<\bar{u}>}{Dt} = -g\frac{dn<\bar{h}>}{dy} + \frac{1}{\rho}\mu\frac{\partial^2 nU}{\partial z^2} + \frac{1}{\rho}\frac{\partial n\tau_{yz}}{\partial xz} + \upsilon\frac{\partial}{\partial z}n\frac{\partial <\bar{u}>}{\partial z} - D_y \quad , \tag{2.5}$$

Wherein the brackets indicate the spatial average and the over-bar indicates the temporal average. The first term in RHS of equation 3.5 is the pressure difference between upstream and downstream of vegetation. The second term indicates the viscous stress. The third term represents the turbulent shear stresses. Because the turbulent stress is usually much larger than the viscous stress, the second term can be neglected (Buckman, 2013). The fourth term indicates the vertical variation of viscous stress. Within the vegetation patch($x < 0$), the last term D_y is a function of the vegetative drag and bed friction factor c_f in case of a vegetation patch adjacent to a main channel. In the main channel ($x > 0$), the drag is only a function of the bed friction c_f . X-coordinate is defined that $x = 0$ is at the interface of vegetation patch and main channel and positive towards the main channel.

$$D_y = \begin{cases} \frac{1}{2}\rho(C_D a + \frac{c_f}{h})U^2, x<0 \\ \frac{1}{2}\rho(\frac{c_f}{h})U^2, x>0 \end{cases} \tag{2.6}$$

2.2 Stem scale and canopy scale turbulence

When flow passes a patch of emergent vegetation, the turbulence level depends on the stem Reynolds number $Rd = \frac{Ud}{\upsilon}$. If $R_d \geq 100$, the stem scale vortices are formed (Nepf, 2012b). When the vegetation density is low, the wake produced due to passing flow is the main cause of energy dissipation. When the stem density is high that the averaging space between stems is smaller than stem diameter, the stem-scale turbulence is further limited by the space between stems.
The Canopy scale turbulence starts to play a role when the density of stems is high enough to influence the momentum exchange between main channel and vegetation patch. The shear mixing layer formed at the flow-vegetation interface features rapidly changing flow velocity. The shear mixing layer is divided into two parts: inner layer penetration length δ_I and the outer boundary length δ_0 in the main channel.

The length of the inner layer and outer layer can be estimated by the maximum drag length scale and the stem diameter (White, Brian and Nepf, Heidi, 2008) :

$$\delta_I = \max(0.5(C_D a)^{-1}, 1.8d)$$

$$\delta_0 \sim \frac{u_*^2}{U_2^2}\frac{2h}{c_f} \tag{2.7}$$

In which $u_*^2 = -<\overline{u'v'}>_{\max}$ is defined as the maximum Reynolds stress at the vegetation-flow interface; U_2 is the free flow velocity in the main channel which is not influenced by the vegetation.

2.3 (Rigid) 3D Vegetation model

For the purpose of studying the effects of vegetation on flow behavior and turbulence, Uittenbogaard (dec.2000) developed a theory to include the effects of vegetation on momentum and turbulence equations and applied this in the '(Rigid) 3D Vegetation model'. This model can also be used in 2DH environment. The application of this model has been calibrated and validated successfully for tidal systems (Temmerman et al., 2005b; Bouma et al., 2007). A brief introduction to the theoretical background of this model is given in this section because the vegetation model is used in this study.

This vegetation model extends the momentum equation with a vertical distribution of vegetation-induced friction force $F(z)$ [N/m^3]:

$$F(z) = \frac{1}{2}\rho_w C_D n(z) D(z) |u(z)| u(z) \tag{2.8}$$

Wherein ρ_w is the water density [kg/m^3]; C_D is dimensionless and represents the cylindrical drag coefficient [-]; $n(z)$ indicates the vertical distribution of number of cylinders per unit are $[m^{-2}]$ with the vertical distribution of stem diameter $D(z)$ [m]; $u(z)$ is the depth-dependent horizontal velocity[m/s].

Once taking into account the effects of vegetation, momentum exchange is influenced by the porosity of of the vegetation $(1 - A_P(Z))$ where $A_p(z)$ is the horizontal cross sectional vegetation area :

$$A_p(z) = \frac{1}{4}\pi D^2(z) n(z) \tag{2.9}$$

The vegetation effects are included in the momentum equation through the eddy viscosity ν [m^2/s], which is solved by $k-\varepsilon$ turbulence model. This model is modified to calculate (i) the turbulence and dissipation generated by vegetation and (ii) The turbulence diffusion with decreased horizontal cross sectional area $(1 - A_p(z))$ (Uittenbogaard, 2003).

The vegetation effects influence the vertical fluctuations through an extra source term T in the kinetic energy equation (Deltares, 2016):

$$\frac{\partial k}{\partial t} = \frac{1}{1 - A_p}\frac{\partial}{\partial z}\{(1 - A_p)(\nu + \frac{\nu_t}{\sigma_k})\frac{\partial k}{\partial z}\} + T + P_k - B_k - \varepsilon \tag{2.10}$$

With k [$N*m$] the kinetic energy; ν_t [m^2/s] is the eddy viscosity; P_k is the production term and ε is the dissipation term; $T(z)$ is the work done by the fluid per unit time [$N*m/s$]:

$$T(z) = F(z)u(z) \tag{2.11}$$

Also another extra source term $T\tau^{-1}$ is added in the epsilon equation (Deltares, 2016):

$$\frac{\partial \varepsilon}{\partial t} = \frac{1}{1-A_p}\frac{\partial}{\partial z}\{(1-A_p)(\nu + \frac{\nu_t}{\sigma_k})\frac{\partial \varepsilon}{\partial z}\} + T\tau^{-1} + P_\varepsilon - B_\varepsilon - \varepsilon_\varepsilon \quad (2.12)$$

With τ the minimum time scale:

$$\tau = \min(\tau_{free}, \tau_{veg}) \quad (2.13)$$

With the dissipation time scale of free turbulence τ_{free} and eddies within vegetation τ_{veg} :

$$\tau_{free} = \frac{1}{c_{2\varepsilon}}\frac{k}{\varepsilon}, \tau_{veg} = \frac{1}{c_{2\varepsilon}\sqrt{c_\mu}}\sqrt[3]{\frac{L^2}{T}} \quad (2.14)$$

Wherein L is the representative length restricted by the smallest distance between vegetation:

$$L(z) = C_l\sqrt{\frac{1-A_p(z)}{n(z)}} \quad (2.15)$$

C_l is a length scale coefficient for reducing the geometrical length scale to turbulence length scale. Uittenbogaard (dec.2000) suggests a C_l value of 0.8 is recommended for vegetation.

2.4 Wall roughness

The presence of wall (closed boundaries) slows down the flow near the wall and the momentum exchange leads to the formation of boundary layer. The boundary layer is the area which is affected by the presence of closed boundaries. The kinetic energy in the flow and turbulent eddies transformed into heat due to the shear stress along the wall. The shear stress along the boundary in an uniform flow is defined based on logarithmic law:

$$\tau_b = c_f \rho \overline{\overline{u}}^2 = \rho {u_*}^2 \quad (2.16)$$

Wherein the c_f is the dimensionless friction coefficient; u_* is known as the shear velocity :

$$u_* = \sqrt{\tau / \rho} \quad (2.17)$$

The shear velocity is actually a shear stress parameter with a dimension of velocity. It can not be measured in reality. The Chezy and Manning coefficients are defined as:

$$C = \sqrt{\frac{g}{c_f}} \quad \text{and} \quad n = R^{1/6}\sqrt{\frac{c_f}{g}} \tag{2.18}$$

A combination of equations (2.3.1) and (2.3.3) leads to another expression of u_* :

$$u_* = \overline{\overline{u}}\sqrt{g}/c \tag{2.19}$$

The Chezy coefficient can also be written as a function of bed roughness length:

$$C = 18\log(\frac{12H}{k_s}), k_s = 30z_0 \tag{2.20}$$

In which z_0 is the roughness length [m]; k_s is the geometrical roughness of Nikuradse.

In order to gain an uniform and fully developed flow, a distance equal to 30-50 times the water depth is needed to reach equilibrium state . The thickness of the boundary grows with $\delta(x) \approx 0.02x$ to $0.03x$ (Schiereck and Gerrit J, 2012), in which x is positive towards the stream-wise direction. In case of acceleration and deceleration flow. The boundary layer changes with a rate estimated by :

$$\frac{d\delta}{dx} = \frac{-(4to5)\delta}{u_0}\frac{du_0}{dx} \tag{2.21}$$

Indicating that acceleration of flow reduces the thickness of boundary layer and deceleration is the other way around.

In Delft3D, two boundary conditions are prescribed at the closed boundary. One is the flow normal to the boundary and the other is the shear stress along the boundary . The boundary condition of the former one is no flow through the boundary and the latter can be a choice among one of the following (Deltares, 2016):

1. Free slip (zero shear stress)
2. Partial slip
3. No (zero velocity at the wall)

In case of large scale simulations, the effects of wall roughness can be neglected so that free slip should be used. For small (flume) scale simulations, the wall roughness plays an important role and partial slip is recommended. The flow velocity near the wall is calculated with (Deltares, 2016):

$$\left|\overline{u}_{sidewall}\right| = \frac{u_*}{\kappa}\ln(1+\frac{\Delta x}{2z_0}) \tag{2.22}$$

In which κ is known as Karman constant with a value around 0.4; Δx is the grid size normal to the wall and z_0 is the roughness length.

2.5 Eddy viscosity

2.5.1 Concept of eddy viscosity

In order to solve the shallow water equations in turbulent flow with limited computer power, many methods are designed such as RANS model (Reynolds-averaged Navier-Stokes) and LES (Large eddy simulation). Using Direct Numerical Simulation Horizontal (DNS) to solve turbulent flow with any flow scales is not possible yet due to limited computer power (VANVossen, 2000). The amount of mesh points needed for DNS is proportional to $\mathrm{Re}^{9/4}$ (Hirt 1969), which requires extremely large computer memory. Delft3D applied the concept of LES because it can solve the equations with reasonable accuracy and the SGS (sub-grid scale) models are less dependent on flow type (Van Vossen,2000).

HLES (horizontal large eddy simulations) is originally designed for the simulations of large scale flow with coarse grids, which is not the case in this study. However, Van Vossen(2000) utilized HLES to simulate flume scale flow and produced valuable results. Therefore, HLES is still a consideration of this study. Also, the concept of eddy viscosity is still important in this study and it will be introduced in this section.

Navier Stokes equations describe the motion of flow and govern the velocity and pressure of a viscous flow. In this equation, each part can be decomposed into a average term and fluctuating term. Averaging the Navier Stokes equations leads to the RANS equations. However, nonlinear term $-<U_i^{'}U_j^{i}>$ still exists in the convection term. This is called Reynolds stress term and the difficulties in modeling this term is known as closure problem. The concept of eddy viscosity is firstly introduced to solve the closure problem in RANS equations. The depth averaged RANS momentum equation reads (Van Vossen,2000):

$$\frac{\partial <U_i>}{\partial t}+<U_j>\frac{\partial <U_i>}{\partial x_j}=-g\frac{\partial <\xi>}{\partial x_i}+<F>-\frac{\partial <T_{ij}>}{\partial x_j}+\frac{\partial <I_{ij}>}{\partial x_j} \qquad (2.23)$$

In which F represents the Coriolis force; $<T_{ij}>$ is known as the Reynolds stress term and it can be written as:

$$<T_{ij}>=<U_i^{'}U_j^{'}> \qquad (2.24)$$

The concept of eddy viscosity is introduced by (see e.g. Batchelor, 1967):

$$-<U_i^{'}U_j^{'}>=2v_T<D_{ij}>-\frac{1}{\rho}<P_t> \qquad (2.25)$$

With the average turbulent pressure:

$$<P_t>=\frac{1}{3}<u_k^{'}u_k^{'}>\delta_{ij} \qquad (2.26)$$

Wherein ν_t is the eddy viscosity and it is proportional to the Reynolds stress term. In Delft3D, HLES is used to calculate the SGS(sub-grid scale) horizontal eddy viscosity ν_{SGS} that are not resolved by the horizontal grid. ν_H^{back} is a user-defined background viscosity used to represent the turbulent forcing that is not resolved by RANS equation. The horizontal eddy viscosity is a combination of different terms (Deltares,2016):

$$\nu_H = \nu_{SGS} + \nu_v + \nu_H^{back} \tag{2.27}$$

The 3D component υ_v represents the 3D turbulence and it is computed by a 3D turbulence closure model. The vertical eddy viscosity reads:

$$\nu_v = \nu_{mol} + \max(\nu_{3D}, \nu_v^{back})$$

with ν_{mol} the kinematic viscosity of water and ν_{3D} is computed by a 3D turbulence closure model. Table 2.1 is an overview of eddy viscosity options in Delft3D-Flow.

Table 2.1: Overview of eddy viscosity options in Delft3D-Flow (Deltares,2016)

Model description	υ_{SGS}	υ_H^{back}	υ_{3D}	υ_v^{back}
2D, no HLES	-	2D-turbulence +dispersion coefficient	-	-
2D, with HLES	Computed by HLES	3D-turbulence +dispersion coefficient	-	-
3D, no HLES	-	2D-turbulence	Computed by vertical turbulence model	Background vertical viscosity
3D, with HLES	Computed by HLES	-	Computed by vertical turbulence model	Background vertical viscosity

It should be noticed that the background horizontal eddy viscosity plays an important role since it represents different meanings in different scenarios. The models used in this study belongs to the first row of Table 2.1 so that the HLES model is not used. The detail of HLES model is still given in section 2.5.3 to give a reason why the HLES model is not used in this study.

2.5.2 Horizontal Reynolds Stress

It is well known that the coherent eddy structures developed at the shear mixing layer have a larger spatial and temporal scale than those of the bottom induced turbulence (for example Uijttewaal 2002). If the contribution from advective dispersion is neglected, the momentum exchange occurs in the shear mixing layer is caused by the depth averaged turbulent shear stress : $T_{xy} \approx -\rho < \overline{u'v'} >$. The concept of eddy viscosity is introduced to determine the horizontal Reynolds stress :

$$-<\overline{u'v'}>= v_t \frac{d\overline{U}}{dy} \tag{2.28}$$

In which v_t is the eddy viscosity and y is in cross shore direction. According to Wormleaton (1988), the eddy viscosity can be divided into two components: a contribution from bottom turbulence $(v_t^{'})$ and the other from large scale horizontal coherent structures $(v_t^{''})$:

$$v_t = v_t^{'} + v_t^{''} \tag{2.29}$$

The bottom induced turbulence $v_t^{'}$ can be calculated by 3D $k-\varepsilon$ model and the eddy viscosity $v_t^{''}$ caused by large scale horizontal coherent structures is the main contributor to the background horizontal eddy viscosity v_H^{back}. Regarding the bottom turbulence part, the Elder formula is adopted (van Prooijen et al 2005):

$$v_t^{'}(y) = \alpha D\sqrt{c_f}\overline{U} \tag{2.30}$$

In which D is the water depth and α is a constant with an order of 10^{-1}. The effect of horizontal coherent structures on the momentum exchange is included through Prandtl's mixing length model (van Prooijen et al 2005):

$$v_t^{''}(y) = \beta^2\delta^2\left|\frac{d\overline{U}}{dy}\right| \tag{2.31}$$

In which β is a proportionality constant in the range of 0.088-0.124. δ is the width of mixing layer and it can be estimated with:

$$\delta = 2(y_{75\%} - y_{25\%}) \tag{2.32}$$

$$\overline{U}(y_{25\%}) = \overline{U_f} + 0.25(\overline{U_c} - \overline{U_f})$$

$$\overline{U}(y_{75\%}) = \overline{U_f} + 0.75(\overline{U_c} - \overline{U_f})$$

In which U_c is the flow velocity in the main channel and U_f is the flow velocity at the floodplain.

Equation (2.5.2.4) does not take into account the lateral depth variation and it actually plays a role for large scale eddies. Considering the continuity the lateral velocity of the eddies increase roughly inversely proportional to the local water depth (1/D(y)) (van Prooijen et al 2005). This concept is illustrated in Figure 2.1.

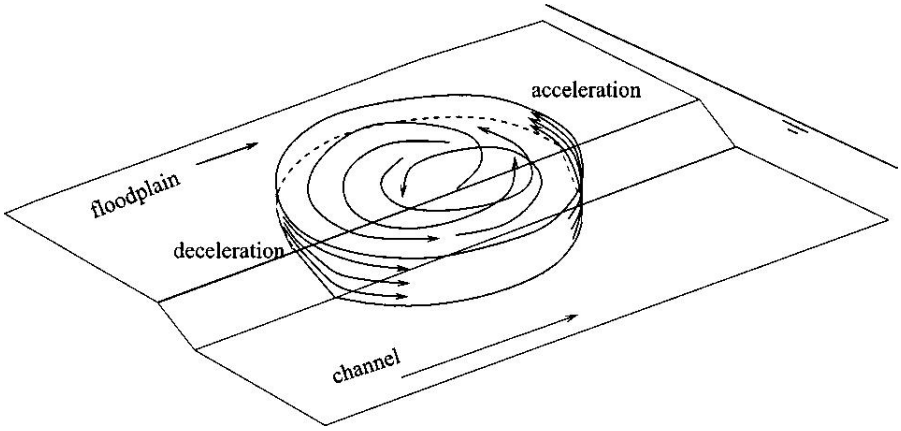

Figure 2.1: Sketch of eddy moving on slopy bottom (van Prooijen et al 2005).

In order to include the effect of water depth, equation 2.31 is modified:

$$v_t''(y) = \frac{D_m}{D(y)} \beta^2 \delta^2 \left| \frac{d\overline{U}(y)}{dy} \right| \tag{2.32}$$

In which D(y) is the local water depth and $Dm = (D_c + D_f)/2$.

2.5.3 Horizontal large eddy simulations

The concept of large eddy simulations(LES) is to compute only the large scales of the flow and cut off the small scales. The large scale flow should be computed as in direct numerical simulations(DNS) and the small scale flow is computed by a SGS model (Van Vossen, 2000). This method can be justified by the fact that the main behavior of the flow is mainly determined by large eddies. In Delft3D, HLES model can be used to calculate the horizontal component of the SGS eddy viscosity and eddy diffusivity. The theory of HLES is first presented by Uittenbogaard (1998). The SGS eddy viscosity υ_{SGS} reads (Deltares, 2016):

$$\nu_{SGS} = \frac{1}{k_s^{\,2}}(\sqrt{(\gamma\sigma_T S^*)^2 + B^2} - B) \tag{2.33}$$

With: $B = \dfrac{3g|\vec{U}|}{4HC^2}$ (2.34)

where C is the Chezy coefficient and H is the water depth. The coefficient B represents the damping caused by bottom friction. As can be seen from equation 2.34, a shallow water depth combined with a rough bed can leads to a large value of damping coefficient B, which suppressed the SGS eddy visocisty. More detail is given in Figure 2.3. Also, the sub-grid eddy diffusivity reads :

$$D_{SGS} = \frac{\nu_{SGS}}{\sigma_T} \tag{2.35}$$

The S^* in equation (2.4.4) indicates the sum of strain rates squared (for more details, see (Van Vossen,2000)):

$$(S^*) = 2(\frac{\partial u^*}{\partial x})^2 + 2(\frac{\partial v^*}{\partial y})^2 + (\frac{\partial u^*}{\partial y})^2 + (\frac{\partial v^*}{\partial x})^2 + 2\frac{\partial u^*}{\partial y}\frac{\partial v^*}{\partial x} \tag{2.36}$$

In case of 3D turbulence the dissipation caused by viscous effects reads:

$$B^{(3D)} = \nu k_f^2 \tag{2.37}$$

Where k_f is the cut-off wavelength which is applied by equation (2.33) (Van Vossen,2000) :

$$k_f = \frac{\pi f_{lp}}{\Delta} \tag{2.38}$$

In which f_{lp} is called the low-pass filter and it can be used to correct the difference between numerical cut-off wave number and theoretical cut-off wave number. Figure 2.2 illustrates the definition of two cut-off wave numbers. The theoretical cut-off wave number is determined by the filter applied and it is an exactly defined number, but the numerical cut-off number depends on the applied scheme and it is arbitrary (Van Vossen,2000). The kinematic energy of flow structures in resolved scales drop rapidly at wave numbers larger than a certain numerical cut-off. This is known as numerical dissipation and it is caused by the spatial discretization (applied scheme). The task of the SGS eddy viscosity model is removing energy from the resolved scale. Therefore, the sum of the numerical dissipation and dissipation of SGS model should equal the theoretical forward scatter (Van Vossen,2000), which is the energy transferred from large scale flow to SGS flow.

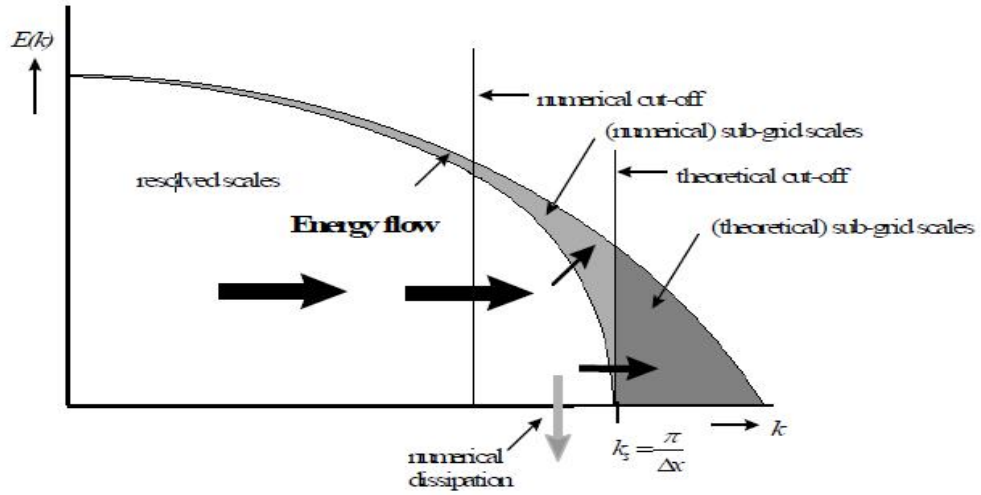

Figure 2.2 : Difference between numerical cut-off wave number and theoretical cut-off wave number (Deltares, 2016).

In Delft3D, the SGS eddy viscosity model depends on the theoretical cut-off wave number instead of the numerical cut-off wave number. So the spatial low pass filter f_{lp} is needed to make SGS model remove more energy from the relatively small wave number. A value of $f_{lp} \approx 0.3$ is recommended according to the simulations of Van Vossen (2000).

Due to the fact that the HLES model is always working together with SGS eddy viscosity model. The applicability of HLES model can be evaluated by introducing the concept of damping of SGS eddy viscosity by bed friction ((Uittenbogaard, R.E., and van Vossen, B., (2004)). Equation 2.33 is rewritten by:

$$\upsilon^{SGS}(B>0) = f(z)\cdot\upsilon^{SGS}(B=0) \tag{2.39}$$

With $z = B/\gamma\sigma_T\sqrt{S^*:S^*}$ and the function

$$f(z) = \sqrt{1+z^2} - z \tag{2.40}$$

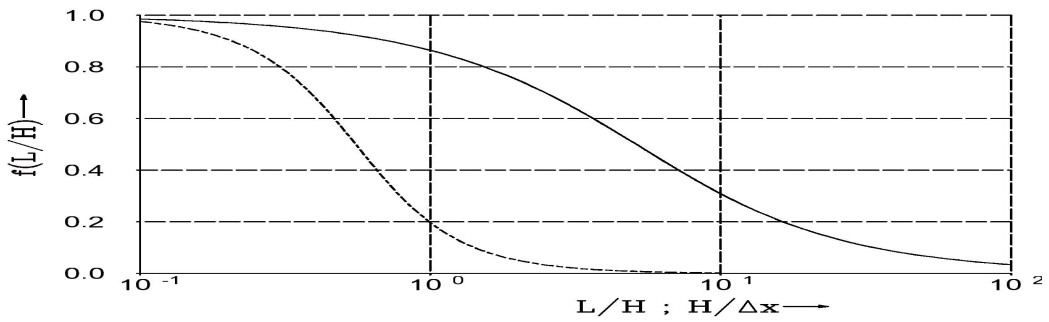

Figure 2.3 : Reduction of υ^{SGS} through bed friction. Dashed line shows a vanishing SGS eddy viscosity for L=10H ((Uittenbogaard, R.E., and van Vossen, B., (2004)).

In this study , the ratio of eddy size (L) over the water depth (H) is around 1 m/0.1 m=10. The dashed line can be used to estimate the damping of SGS eddy viscosity. With a water depth between 0.04 and 0.12 m and a minimum grid size of 0.02 m, the valule of $H/\Delta x$ lies between 2 and 6, which leads to a value of f(L/H) smaller than 0.2. Therefore, the SGS eddy viscosity is much damped and the HLES model is hardly dependent on the SGS eddy viscosity model. Also, the resolved part of HLES model more or less solves the same thing as the RANS model, since the averaging behavior of the flow mainly depends on the behavior of the large scale flow. Therefore, the use of HLES model in this study is not necessary.

2.6 Summary

The theory behind this study covers a wide range of subjects. The flow pattern in this study is influenced by the combined effects of bed roughness, emergent vegetation, and turbulence, etc. This chapter only gives a background needed for explanation of the model and experimental results. This study will mainly focus on the application of the model and the explanation of the results.

The literature until now either focuses on the understanding of the physics in partially vegetated channel by conducting experiments or purely on the numerical model. This study combines this two fields and explore the limitation of Delft3D to simulate the flow velocity profile and to capture the eddy structures. This is the basis of this study. The approach, results and conclusions are presented in the following chapters.

Chapter 3

3.1 Introduction

Numerical model functions as a tool to study the hydrodynamics around mangroves at a higher spatial and temporal resolution and scale than flume experiments. Also, the set up of numerical model is flexible and time-saving. It improves our understanding of the flow characteristics in a partially vegetated compound channel. In this study, the RANS model in Delft3D-Flow is utilized to study the physics in a partially vegetated compound channel.

This chapter includes the approach and analysis of this study. Section 3.2 gives a brief introduction of the flume experiments, of which the results are used in this study. Section 3.3 summarizes the model set up and the model results after calibration. The calibration of the numerical model is a process of iteration and the detail is presented in Section 3.4, which also analyzes the influence of different physical parameters (e.g. Bed roughness and drag coefficient) on the flow characteristics. Section 3.5 analyzes the model results of different environmental settings, which include different vegetation density and sloep angle.

3.2 Flume experiments

The flume experiments were conducted by Son(2017). The main purpose of the flume experiments is to capture the physics of momentum exchange between main river channel and mangroves through mixing shear layer. Because the experimental results are be used in this study to combine with the numerical model, a brief introduction of the flume experiments is necessary. This section gives a brief introduction to the flume design and experimental results.

3.2.1 Flume design

The prototype of the experiments is Tiue estuary in Vietnam. Due to the difficulties in implementation of undistorted experiments, only un-scaled experiments were conducted. However, several requirements are met in order to ensure the most important physical processes remain unchanged and can be captured in the experiments. Firstly, a 1/10 slope is adopted, which is the same slope as in the prototype. Secondly, the water depth in the floodplain is at least 5 cm. Thirdly, the Reynolds number should be as large as possible.

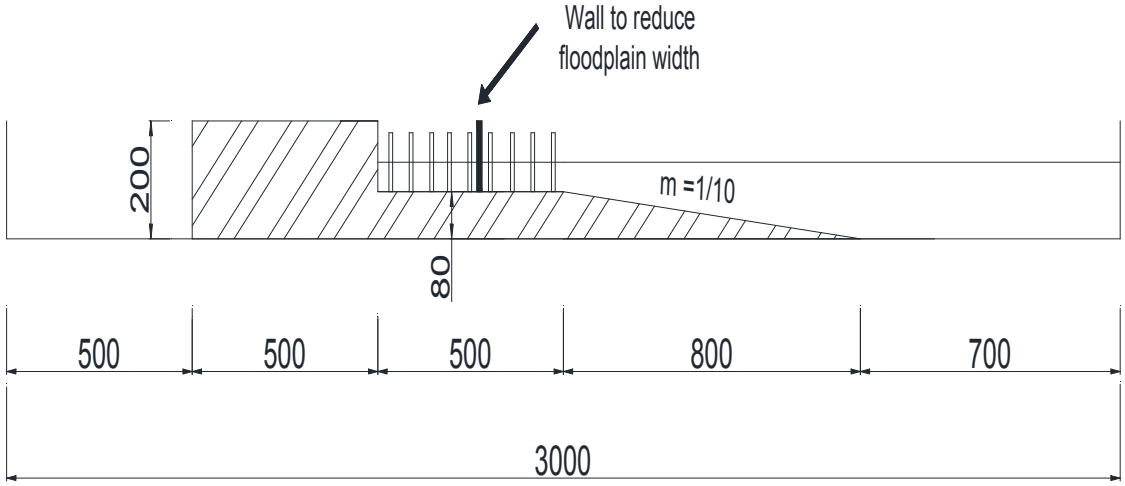

Figure 3.1: Cross sectional profile of the flume. Cylinders represent the mangroves and slope angle is 1/10, which is a typical slope in Mekong estuarine systems.

Figure 3.1 shows a cross section of the flume. The flume is 3 meters wide but water only flows in the area with a width of 2 meters. The cylinders on the flood plain represent the mangroves. The height of the cylinders is 10 cm and different densities are applied in the experiments. The wall is used in the experiments to adjust the width of the floodplain.

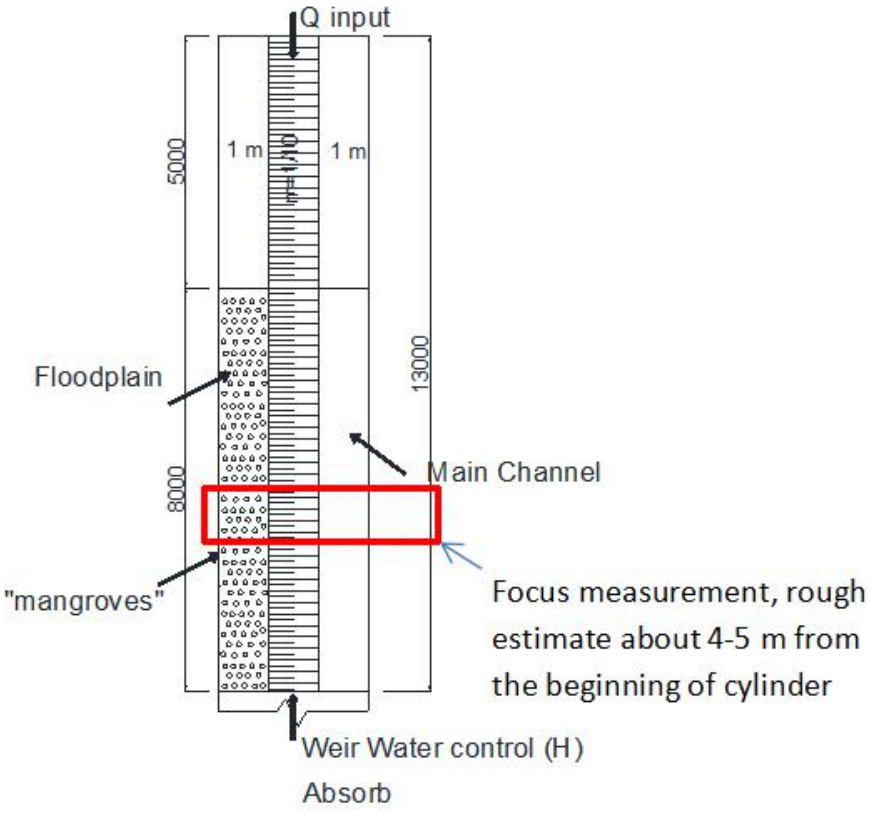

Figure 3.2: Plan view of the flume. A constant discharge is applied in upstream and a constant water level is applied in the downstream side.

Figure 3.2 shows a plan view of the experiment set up. The dimension of the flume is 3 x 20 meters. The flume is zero-sloped in the stream-wise direction. Discharge can be adjusted on the upstream side and water level can be controlled on the downstream side. The flow velocity is measured around 4.8 meters from the beginning of cylinders by ADV so that a velocity profile along a cross section can be captured. More than 20 measurement points are employed along the cross-shore section. The velocity is measured at the middle of the water depth so that the measured velocity is close to depth-averaged velocity. The reason why velocity is measured 4.8 meters from beginning of cylinders is that flow needs a distance to reach the equilibrium condition. So after 4-5 meters the flow is fully developed. The cylinders are arranged in a staggered way . There are two different densities with sparse vegetation (139 cylinders/ m^2) and dense vegetation (139 cylinders/ m^2).

Figure 3.3 shows the flume where the experiments were conducted.

Figure 3.3: The flume experiments are conducted with dyes. The flume is zero-sloped with cylinders on the floodplain. The velocity is measured by ADV along a cross section around 4.5 meters from the beginning of the cylinders.

There are four main variables in the experiments: upstream discharge, downstream water level, density of cylinders and width of floodplain. During the experiments, different scenarios were tested. Table 3.1 summarizes all the experiment scenarios. Regarding the upstream discharge, it should be noticed that the discharge is not constant during the experiments due to error of the pump. The deviation is around +/- 5%. So the actual discharge for 45 l/s , for example, could be 42-48 l/s. Hence In the numerical model , the discharge may also be adjusted slightly.

Table 3.1: Summary of all the experiment scenarios.

ϕ	Density 1	Density 2	Density 3
Cylinder/m^2	0	139	550
Q input [l/s]	45,60,80	45,60,80	45,60,80
H control [cm]	12,13,14 cm	12,13,14 cm	12,13,14 cm
Floodplain width [m]	0,5 m ;0.25m ; 0.1 m	0,5 m ; 0.25; 0.1 m	0,5 m ; 0.25 m; 0.1 m

3.2.2 Experimental results

In order to combine the results from flume experiments and numerical model, the experimental results are plotted in the same coordinate with the model. The experimental results are from Son(2017). A series of experiments were conducted for one case so that the results presented below are ensemble-averaged rather than a single realization. The results represent the average behavior of the flow. The results of three typical scenarios are presented below and others can be found in Appendix.

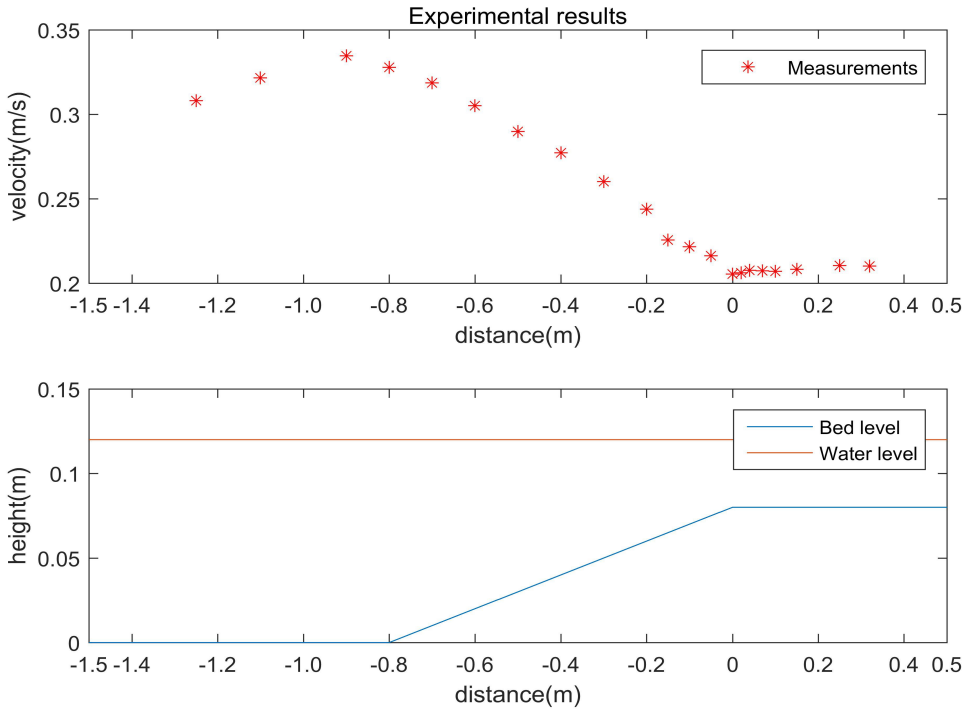

Figure 3.4: Experimental results of 45 l/s discharge, 12 cm water level, 0.5 m floodplain width without cylinders. The velocity is measured at 4.8 meters from the beginning of cylinders. The x-coordinate "0" corresponds to the edge of floodplain.

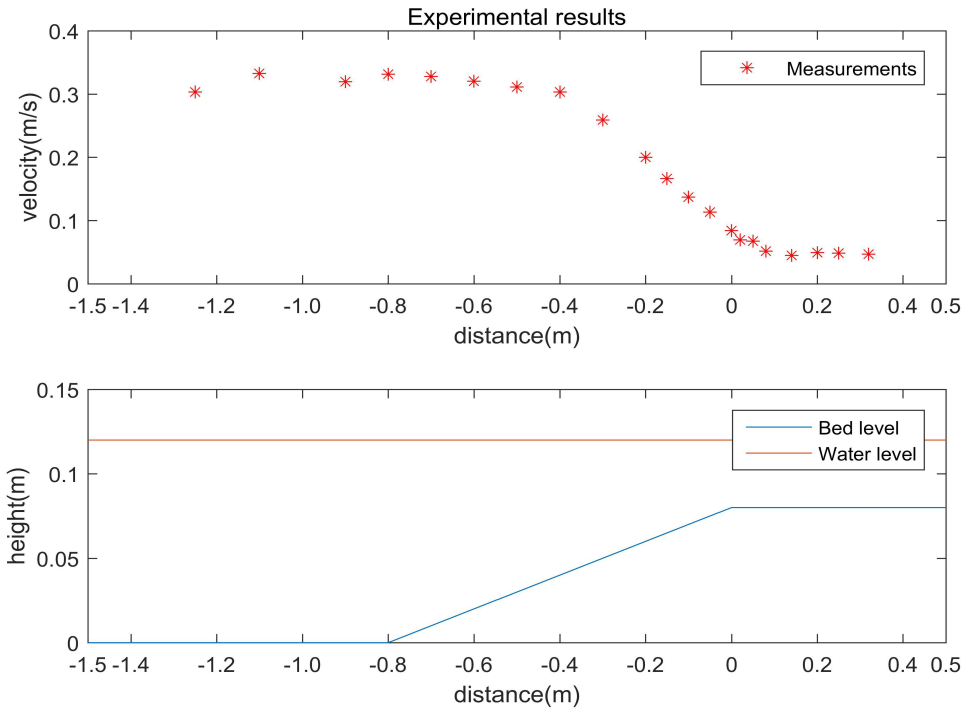

Figure 3.5: Experimental results of 45 l/s discharge, 12 cm water level, 0.5 m floodplain width with sparse cylinders (139 cylinders/ m^2). The velocity is measured at 4.8 meters from the beginning of cylinders.

Figure 3.4 shows the experimental results without cylinders while Figure 5 shows the results with sparse cylinders. It can be seen that the flow velocities reduce rapidly near the floodplain in both figures. In Figure 3.5 the flow velocities on the floodplain are much lower than those in Figure 4 due to the dampening effects of vegetation. While the flow velocities in the main channel in Figure 3.5 are slightly larger than those in Figure 3.4 because a patch of vegetation acts as an obstacle and water flow is deflected towards the main channel. In the next section, D3D will be used to reproduce the experiments numerically and these experimental results are regarded as reference.

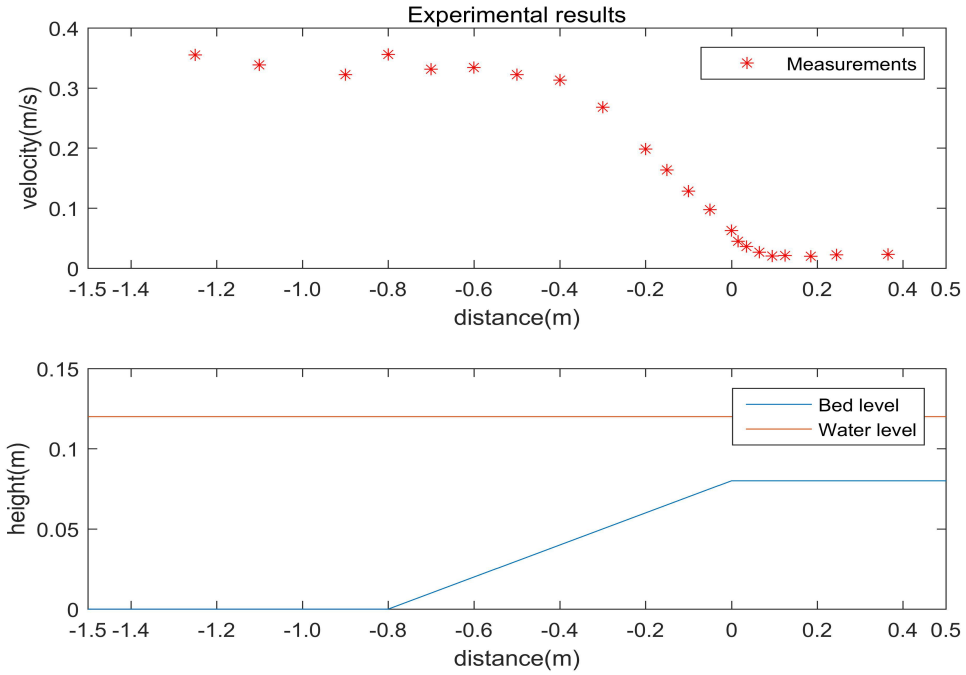

Figure 3.6: Experimental results of 45 l/s discharge, 12 cm water level, 0.5 m floodplain width with dense cylinders (550 cylinders/ m^2).

Figure 3.6 illustrates the experimental results with dense cylinders. Comparing it with Figure 3.5 leads to an observation that the penetration length of the experiment with dense cylinders is slightly shorter than that with sparse cylinders. This is caused by the fact that a dense patch of vegetation damps the flow more efficiently so that the flow velocity drops more steeply near the vegetation patch. Hence the flow needs a shorter length to reach equilibrium. Also, the experiment with dense vegetation is considered as the representative case because the most pronounced coherent structures are observed.

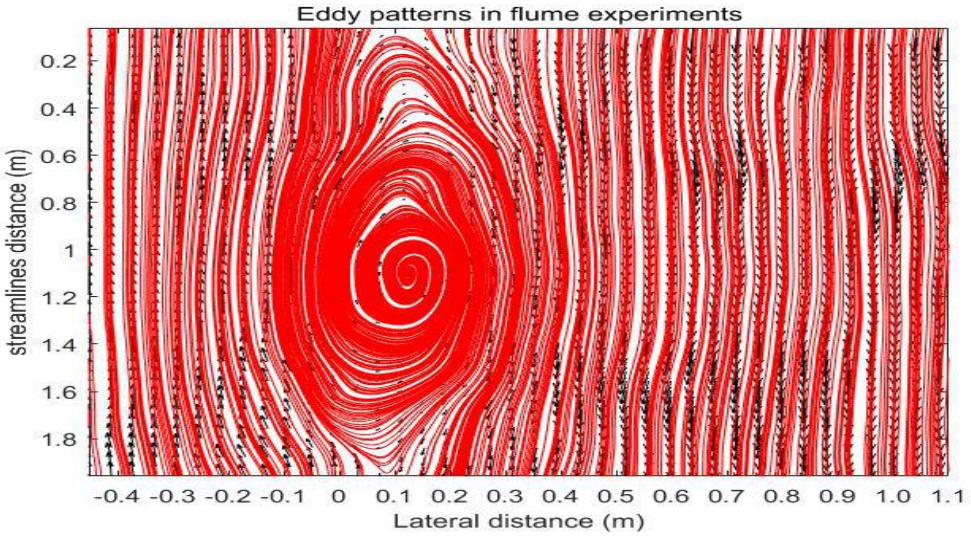

Figure 3.7: Eddy structures observed in experiments with dense vegetation.

As can be seen in Figure 3.7, the width and the length of the eddy are around 0.5 meter and 1.5 meters perspectively. The eddy structure penetrates around 15 cm into the vegetation patch. This eddy pattern is regarded as reference to campared with the model results in next section.

3.3 Model development

The hydrodynamic module Delft3D-FLOW is able to simulate two-dimensional or three-dimensional unsteady flow and sediment transport resulting from tidal or meteorological forcing in shallow water environments (e.g.Temmerman et al., 2005b; Hu et al., 2009). The flow model is applicable in shallow seas, coastal areas, estuaries, lagoons, rivers and lakes. It is designed to model the flow field where the horizontal length and time scales are noticeably larger than the vertical scales (Deltares, 2016). Delft3D-FLOW solves the unsteady shallow water equations in two or in three dimensions. The system of equations includes the horizontal equations of motion, the continuity equation, and the transport equations for conservative constituents. The equations are formulated in orthogonal curvilinear co-ordinates or in spherical co-ordinates. In curvilinear co-ordinates, the free surface level is related to a flat plane of reference, whereas in spherical co-ordinates the reference plane follows the Earth's curvature (for a detailed description, see (Deltares, 2016)).
This section consisits of three parts. Section 3.3.1 introduces the model setup of the reference models(calibrated models) in perspectives of model domain, time frame, boundary conditions and physical parameters. There are two reference models. One is without vegetation and the other is with dense vegetation. They have the same settings except the parameters related to vegetation. A summary of all model settings (including the models for sensitivity tests) is given in Appendix B. Section 3.3.2 gives the results of the reference models and some insights into the model behavior. Section 3.3.3 gives the results of model valiadation.

3.3.1 Model setup

Computational domain

The numerical grid is the grid defining a computational control volume. The depth is defined at the corners of the computational control volume, the numerical grid is drawn through the depth points. Calculations are executed on every numerical grid cell.
Figure 3.8 illustrates the schematized model domain used in this study. The model domain includes a main channel, a 1/10 slope and a flood plain. It should be noticed that the model domain is 4 meters x 20 meters. So after 13 meters behind the mangrove area is a flat area with the same bed level as the main channel and it is 3

meters wide. The grid size varies from 2 cm x 10 cm to 2 cm x 2 cm in the focus measurement area, which is 4-5 meters from the beginning of the cylinders. The water depth in the main channel and flood plain is 12 cm and 4 cm respectively. The ''walls'' at left and right sides of the model domain are 20 cm high so that overflow will not happen and they are impermeable. The model is 2DH so that there is only one vertical layer. This can be justified by the fact that all the vegetation in this study is emergent and there is no variation of vegetation density over the depth. Therefore a 2DH model is sufficient to include the vegetation effects in this study.

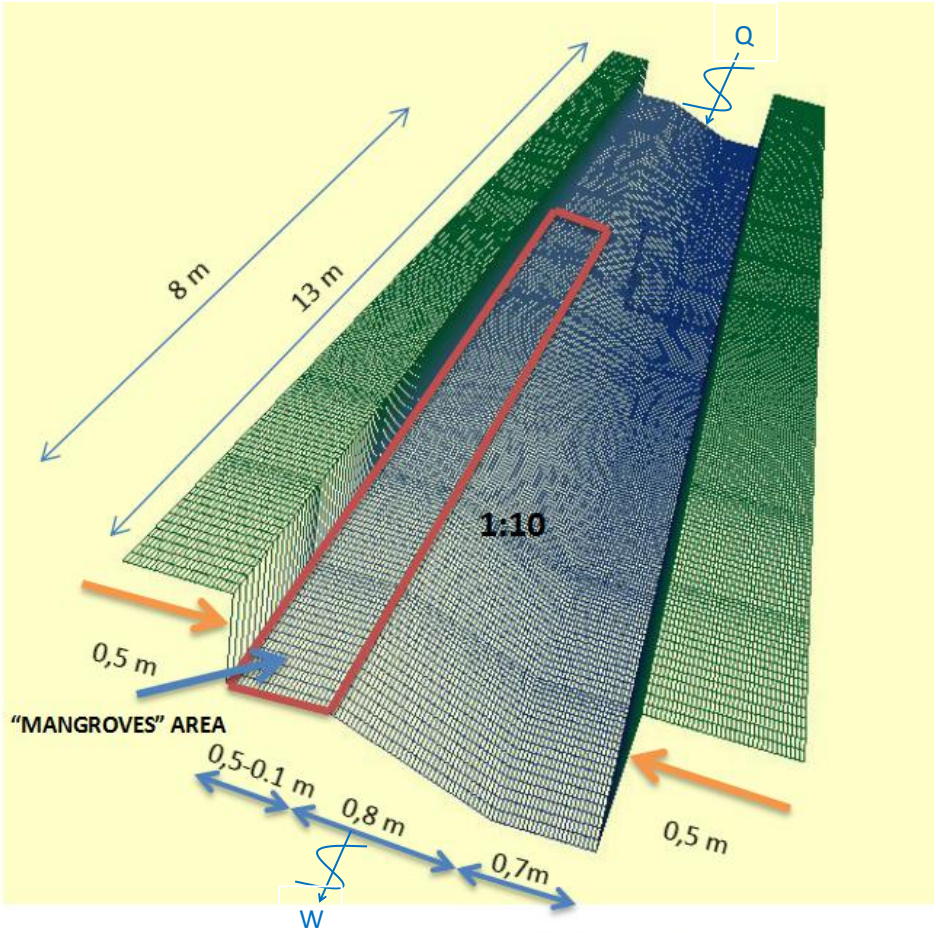

Flume model set up in Delft3D

Figure 3.8: 3D schematized model domain. The model domain includes a main channel, a 1/10 slope and a flood plain.

Time frame

In the Data Group 'Time frame' the time frame of a computation that composed of the reference date, the simulation start time, the simulation stop time and the time step used in the numerical simulation can be specified.

The time step is 0.0001 minute. With a maximun flow velocity around 0.35 m/s the Courant number is around 0.1. This time step is chosen so that the model is stable enough to generate accurate results. The simulation time is 20 minutes.

Boundary conditions

On the upstream side a discharge boundary is chosen with a constant discharge of 0.045 m^3/s . It should be noticed that the width of the whole channel in the upstream is 2 meters and the inflow also covers 2 meters. A water level boundary is prescribed on the downstream side with a constant water level of 0.12 m. The width of the whole channel on the downstream side is 3 meters so that the outflow covers 3 meters. On the water level boundary a reflection parameter alpha is set to 2. The reflection parameter alpha is used to make the open boundary less reflective for short wave disturbances so that the model becomes more stable. However, a excessively large alpha makes the model insensitive to changes of other parameters. The value of alpha can be estimated with (Deltares, 2016):

$$\alpha = T_d \sqrt{\frac{H}{g}} \tag{3.1}$$

In which T_d is the time needed for a free surface wave to travel through the model. With the depth of 12 cm the travel speed is around 1.1 m/s. The length of the model domain is 20 meters so $T_d \approx 18.4s$, which leads to a value of $\alpha \approx 2$.

Physical parameters

Regarding the bed roughness, manning coefficient $[m^{1/3}/s]$ is used and the value is 0.0021 in both reference models. A partial slip condition is used and the roughness length shoule be estimated with equation 2.3.4, 2.3.5 and 2.3.7. These three equations lead to a roughness length in the order of $O(10^{-3})$. After some model tests, a roughness length of 0.002 m is used. A constant background eddy viscosity value of 0.0001 is used in both reference models.

Vegetation input

For the reference model with dense vegetatio $(550/m^2)$, a drag coefficient $Cd = 0.8$ is used. The stem diameter is 0.1 m and the cylinder height is 0.1 m so that all the vegetation is emergent. The vegetation patch starts at 5 meters from the begining of the model and ends at 13 meters. The patch width is 0.5 meter, which is the same width as the floodplain.

3.3.2 Calibration of the model

The calibration of the model in this study bases on the experimental results from Son(2017). Some experimental results are presented in Section 3.2.2 and others are given in Appendix A. The experimental results give the depth-averaged velocity profile in cross-shore direction. The measurements are taken from around 4.8 meters downstream of the beginning of the vegetation patch and there are more than 20 measurement points in cross-shore direction. The calibration of the model focuses on fitting the model results with the experimental measurements.

The calibration of the model consists of two steps. Firstly, the model without vegetation is calibrated. In this step, the calibration mainly focuses on the bed roughness and wall roughness since these are the dominant parameters in flume experiments without vegetation. Secondly, the same model parameters from the previously calibrated model are used as input for the model with vegetation. In this step, the calibration of the model mainly focuses on the drag coefficient and eddy viscosity.

In order to quantify the accuracy of the model results with respect to the experimental results, Nash-Sutcliffe model accuracy MA (Nash and Sutcliffe, 1970) is introduced and applied in this study:

$$MA = 1 - \frac{\sum (SIM - REF)^2}{\sum (REF - \overline{REF})^2} \tag{3.1}$$

In which SIM indicates the model results; REF represents the experimental results and $\overline{REF}$ is the mean value of the experimental results. This formula represents the ratio of squared difference between model and experimental results over the variance of the experimental results. The value of $MA = 1$ represents the perfect match between model and experimental results. If $MA \leq 0$, the model has no predictive skill in addition to the average of the reference data. This model accuracy parameter is frequently used for model simulations of discharge and water quality constituents so that it is also applicable in this study.

Calibration of the model without vegetation

Bed roughness is the dominant parameter in the case without vegetation. The bed roughness in the model should be within a reasonable range according to the calculation from the flume experiments. The bed roughness calculated from the flume experiments is in an order of $O(10^{-3})$ [$m^{1/3}/s$]of manning coefficient. After some sensitivity tests , a manning coefficient of 0.0021 is used in this model. Figure 3.8 shows the calibration of lateral depth averaged velocity profile. The lateral velocity profile is taken at 4.8 m from the beginning of the model. A1 is the name of the reference model without vegetation.

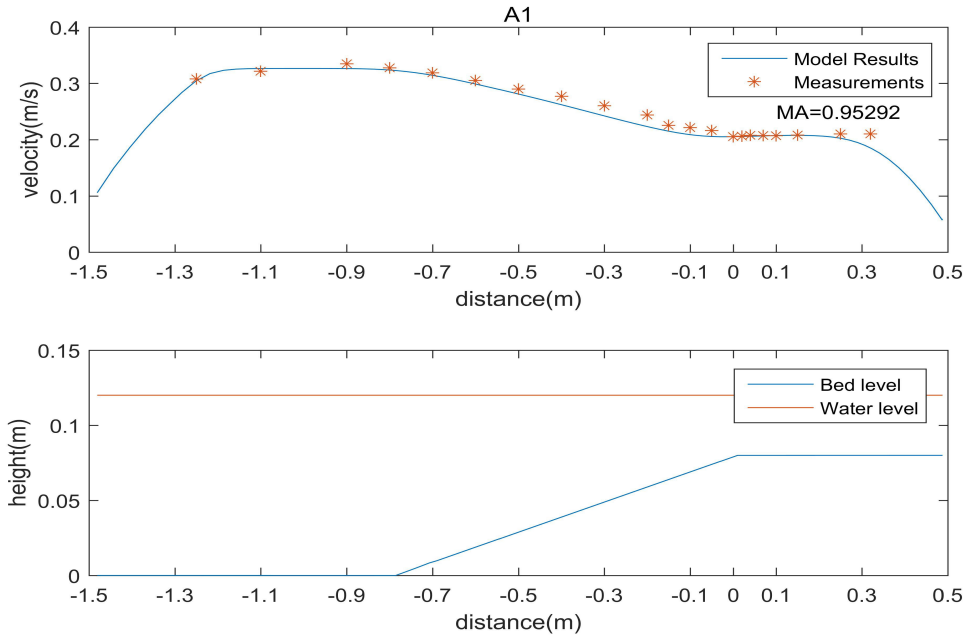

Figure 3.9 : Calibration of the model without vegetation. The upper pannel shows the lateral depth averaged velocity profile. The blue curve is the model results and the red dots are experimental measurements. The lower pannel shows the topography.

As can be seen in Figure 3.10, the model results match well with the measurements overall. Only the velocity on the slope is slightly underestimated. Figure 3.9 shows that no eddy is observed in the model for this case, which is in line with the experimental observation that eddies can be hardly seen.

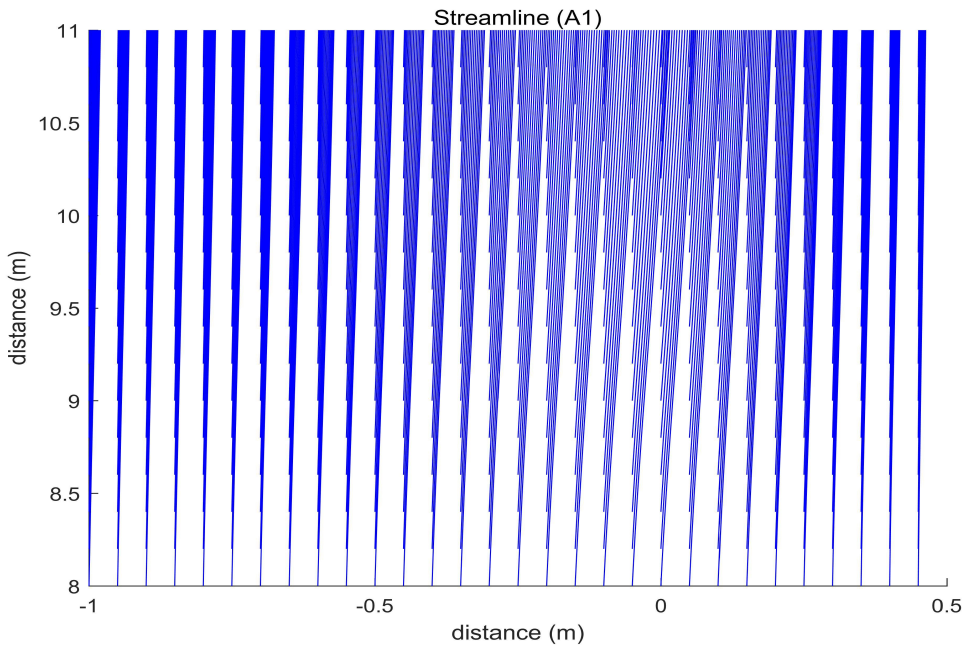

Figure 3.10: Stream line of model A1. X-coordinate “0” corresponds to the floodplain edge. Y-coordinate “8” means 8 meters from the beginning of the model.

Calibration of the model with dense vegetation

The calibration of the model with vegetation mainly focuses on the drag coefficient and eddy viscosity, while keeping other model input the same as the model without vegetation. The sensitivity tests for drag coefficient and background horizontal eddy viscosity are given in section 3.4. Here only the model results are presented.

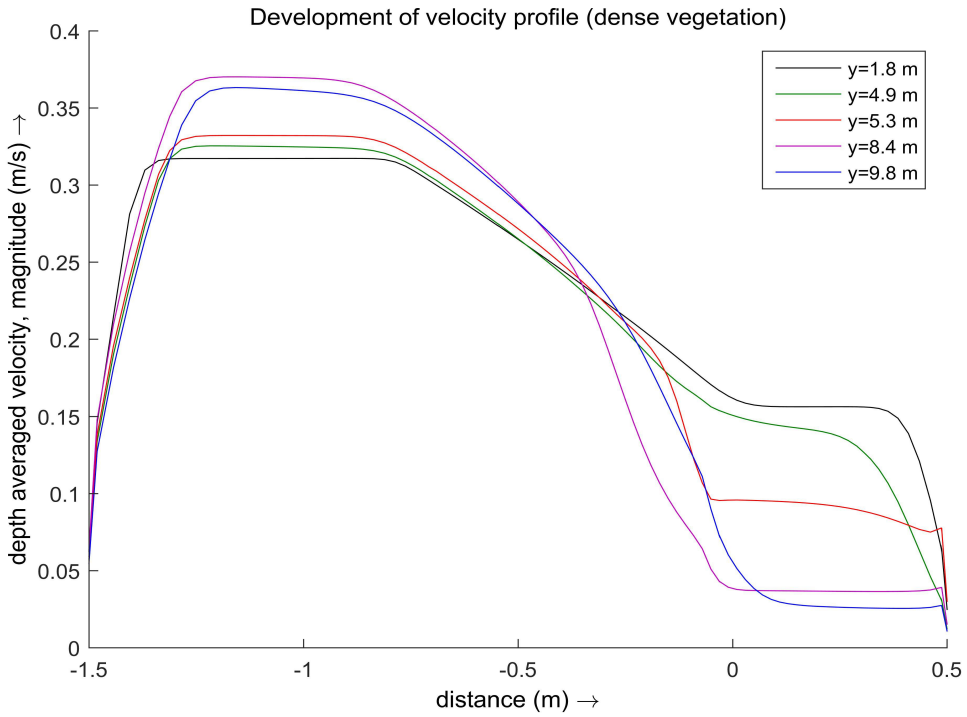

Figure 3.11: Development of lateral depth-averaged velocity profile in streamwise direction. X-coordinate "0" corresponds to the vegetation edge.

When water flow encounters a patch of vegetation, it needs a distance to develop into uniform flow. The model results are taken after this equilibrium has been reached. As can be seen in Figure 3.11, "y" represents the streamwise distance away from the beginning of the model. After 5 meters from the beginning of the model domain, the velocity profile changes rapidly due to the presence of vegetation patch. The flow finally develops into equilibrium at around 9.8 meters, which is 4.8 meters from the beginning of the vegetation patch. This result is in line with the flume experiments where the measurements are taken at around 4.8 meters from the beginning of the vegetation. Therefore the results of model and experiments are compared at the same place.

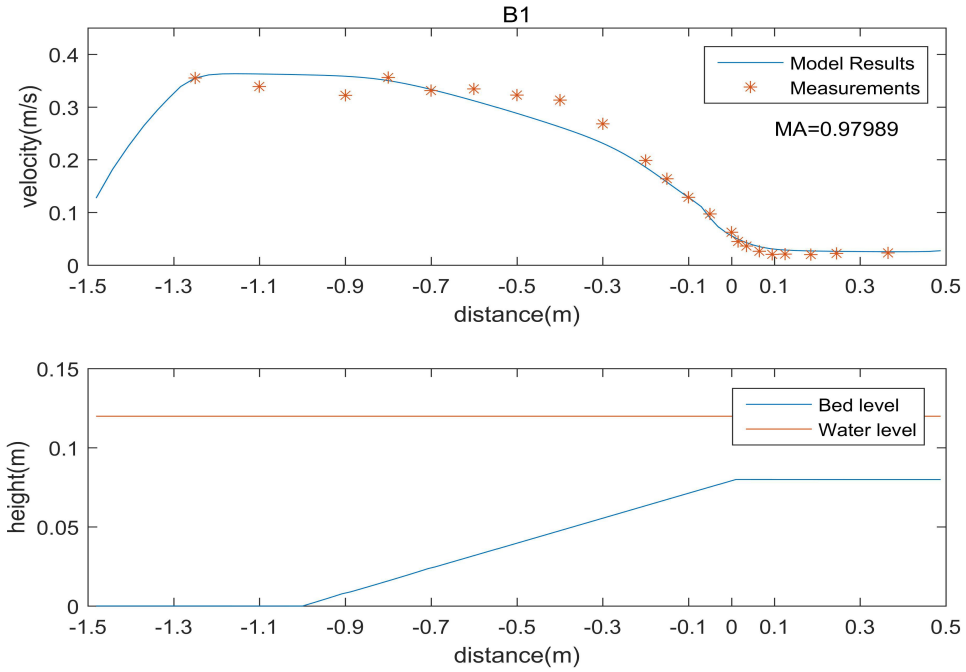

Figure 3.12 : Calibration of the model with dense vegetation. The lateral velocity profile is taken at 4.8 m from the beginning of the model.

Figure 3.12 shows the results of calibrated reference model "B1" with dense vegetation ($550/m^2$). The overall match is good except on the slope where the depth-averaged velocity is underestimated by the model. In order to explain this, a further look into the eddies structures generated from the model is necessary.

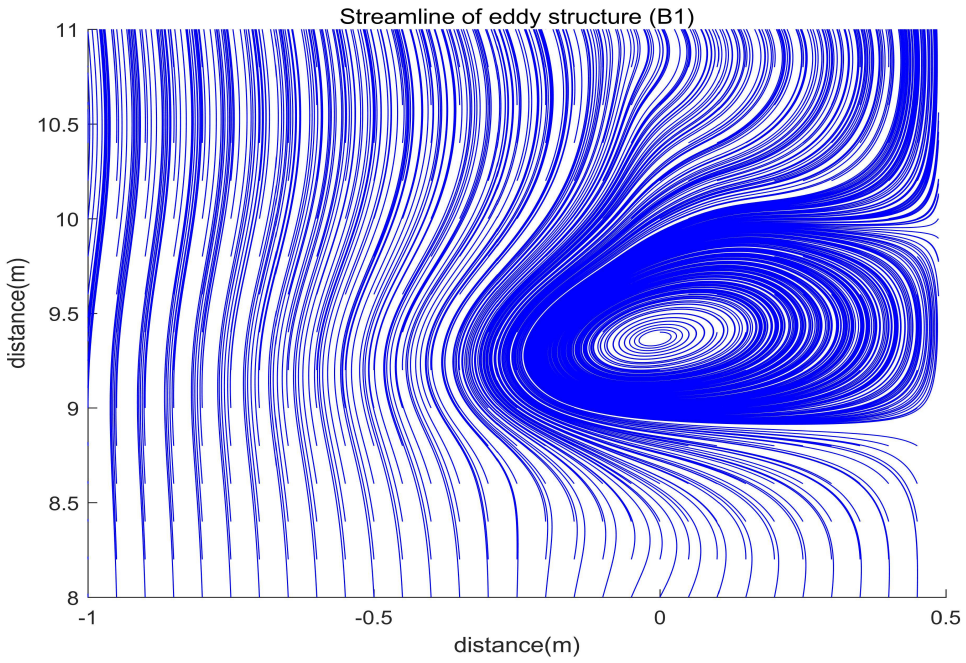

Figure 3.13 : Streamline of eddy structures captured in model B1.

As can be seen in Figure 3.13, the eddy structure fully penetrates into the floodplain. However, according to the observation of the flume experiments in Figure 3.7, only around 15 cm inside the vegetation patch is penetrated by eddies. This might explain the underestimation of the velocity magnitude on the slope: too much momentum is transported into the vegetation patch in the model. However, this explaination might lead to an overestimation of flow velocity magnitude at floodplain. In fact, the flow velocity at the floodplain is well estimated and the drag coefficient is within reasonable range (0.8). In order to have a better understanding of this phenomenon, a further comparison is made between the momentum transport calculated from flume experiments and model results. Figure 3.14

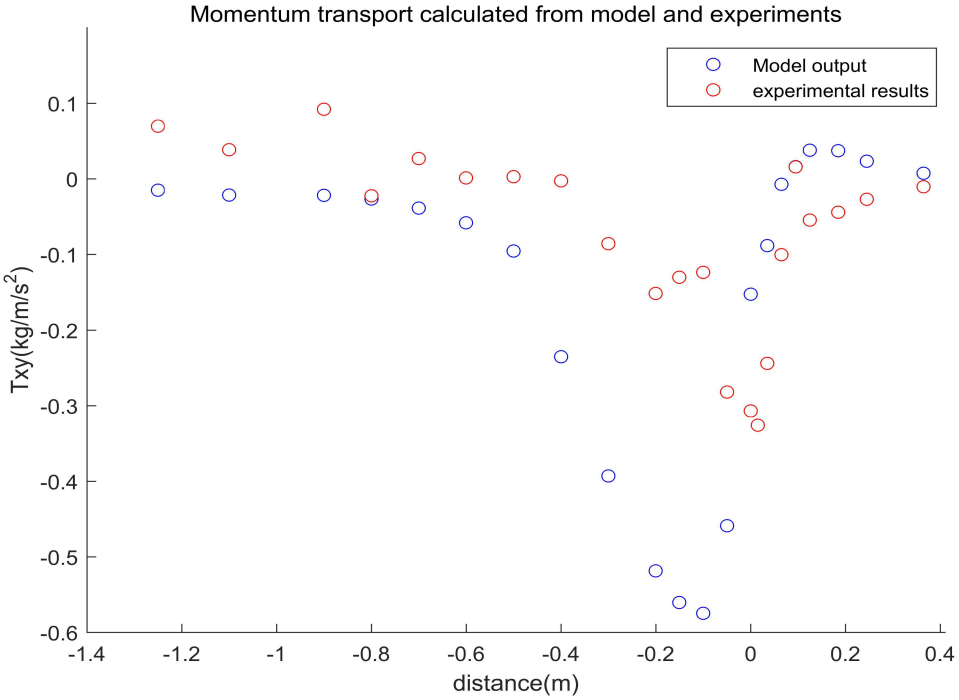

Figure 3.14: Comparison between momentum transport calculated from model output and experimental results.

As can be seen in Figure 3.14, the model output leads to excessive momentum transport in the outer part of shear mixing layer, which can explain the underestimation of flow velocity on the slope by the model as shown in Figure 3.12. However, the model also overestimates the penetration of eddy into the vegetation patch and the penetration of momentum transport calculated from model results is not too much as shown in Figure 3.14. The possible reason is that the eddy structure simulated in the model is not efficient in transporting momentum.

After analyzing the model results, it can be concluded that the model can estimate the global trend of the flow characteristics and the results are resonable. But the model can not reproduce the momentum transport accurately. The possible reason is that the vegetation model only takes into account the overall effects of vegetative drag force instead of considering the effects of each stem. Hence, the stem-scale turbulence is left out by the vegetation model.

3.4 Sensitivity tests

3.4.1 Bed roughness

Bed roughness is the dominant factor in the case without vegetation. Therefore, the calibration of the bed roughness is conducted in the model without vegetation. According to the flume experiments, the bed roughness is in an order of $O(10^{-3})$ [$m^{1/3}/s$]of manning coefficient. Two values of manning coefficient are tested: 0.0021 and 0.0084 $m^{1/3}/s$.

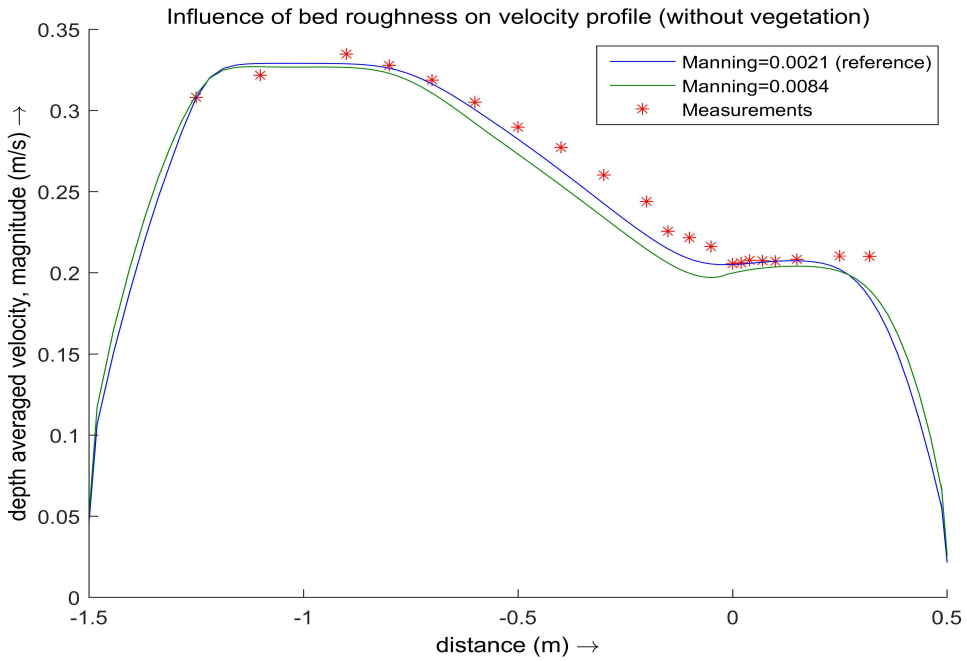

Figure 3.15: Sensitivity test for bed roughness in the case without vegetation.

Figure 3.15 shows that an increasing manning coefficient (rougher bed) leads to a decrease of flow velocity in both main channel and floodplain except the area close to the closed boundaries. This is due to the fact that the discharge is the same in both cases. Therefore, a decreased flow velocity at main channel and floodplain is compensated by an increased flow velocity near the closed boundaries. Also, it can be easily seen that the model results with a manning coefficient of 0.0021 $m^{1/3}/s$ matches better with the experimental results.

In the case of model with vegetation, the effects of bed roughness is overwhelmed by drag coefficient and this can also be proved by Equation 2.6. However, it is found that the bed roughness can influence the eddy structures in the case with vegetation. Therefore, the effects of bed roughness on eddy structures are also tested in the case with dense vegetation.

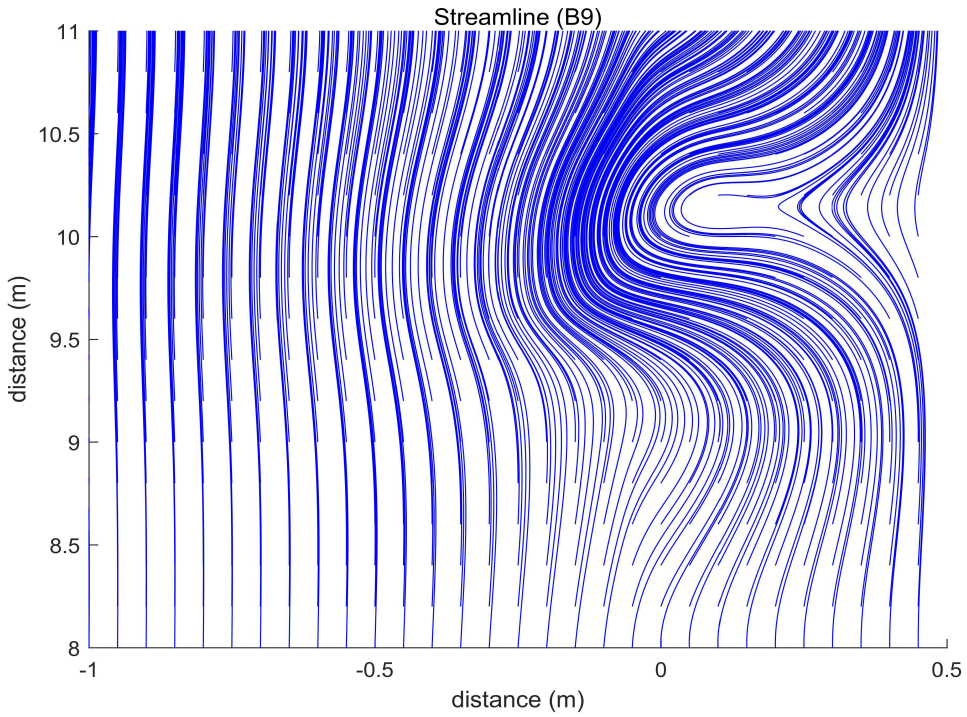

Figure 3.16 : Streamline captured in model B9 (Manning coefficient= 0.0084 $m^{1/3}/s$)

A comparison between Figure 3.13 and Figure 3.16 leads to a conclusion that a rougher bed dampens the energy in the flow and therefore weakens the eddies. However, the eddies observed in the flume experiments are quite strong in the case of dense vegetation. After analyzing the lateral velocity profile and the coherent structures, it seems that a manning coefficient around 0.0021 $m^{1/3}/s$ should be used in this study.

3.4.2 Drag coefficient

When a vegetation patch is considered, the flow decelerates as it approaches the vegetation and accelerates as it leaves. This leads to a pressure difference between the upstream and downstream of the vegetation and increases the drag force on it. The drag coefficients C_D is equal to 1 when a single cylinder is considered. Therefore, the value of drag coefficient should not deviate too much from "1". In this study, three values of drag coefficient are tested in order to find the optimum value to match the measurements : 0.8, 1 and 1.5.

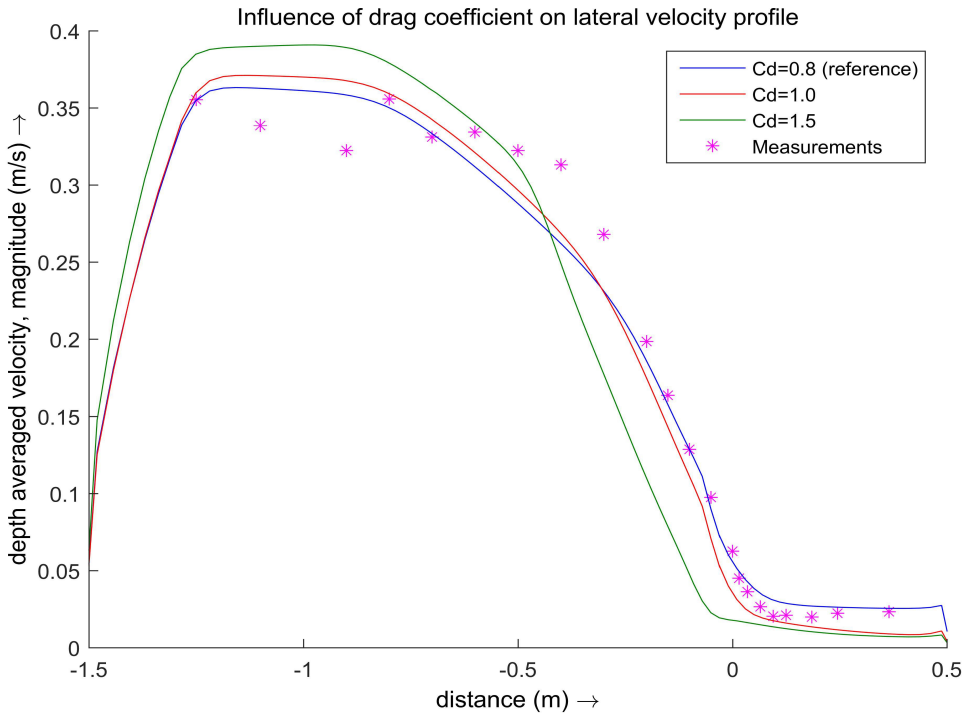

Figure 3.17: Sensitivity test for drag coefficient in the case with dense vegetation. X-coordinate "0" corresponds to the vegetation edge.

When the drag coefficient increases, the vegetation-induced friction also increases. A decrease of flow velocity within the vegetation patch is expected. As can be seen in Figure 3.17, a drag coefficient of 1.5 leads to a much lower flow velocity at floodplain and a higher flow velocity in the main channel. This is because the total discharge is the same in all cases. When the drag coefficient increases, more water flow is deflected into the main channel, which leads to a higher flow velocity in the main channel.

However, it seems that the accuracy of the model with a drag coefficient of 0.8 and 1.0 is hard to compare. Nash-Sutcliffe model accuracy index "MA" described in Equation 3.1 is used to estimate the accuracy of these three models. Table 3.2 summarizes the accuracy of models with three different drag coefficient. Apparently, a drag coefficient of 0.8 leads to a best match with experimental measurements and it is used in the reference model.

Table 3.2 : Accuracy of models with different drag coefficient

Models	Cd=0.8 (B1)(reference)	Cd=1.0 (B10)	Cd=1.5 (B2)
MA	0.9799	0.9731	0.8705

3.4.3 Background horizontal eddy viscosity

As introduced in Section 2.5.2, horizontal eddy viscosity is proportional to the horizontal Reynolds stress $-<\overline{u'v'}>=v_t\frac{d\overline{U}}{dy}$, which is related to the horizontal momentum transport if the advective dispersion is neglected : $T_{xy}\approx-\rho<\overline{u'v'}>$.

Therefore, the flow characteristics within the shear mixing layer are dominated by the horizontal eddy viscosity. In order to generate best results from the model, two ways of inputting background horizontal eddy viscosity are investigated. Firstly, a triangular distribution of horizontal eddy viscosity according to the calculation from flume experiments is tested. Secondly, different uniform values of horizontal eddy viscosity are tested. Figure 3.18 illustrates different ways of inputting background horizontal eddy viscosity.

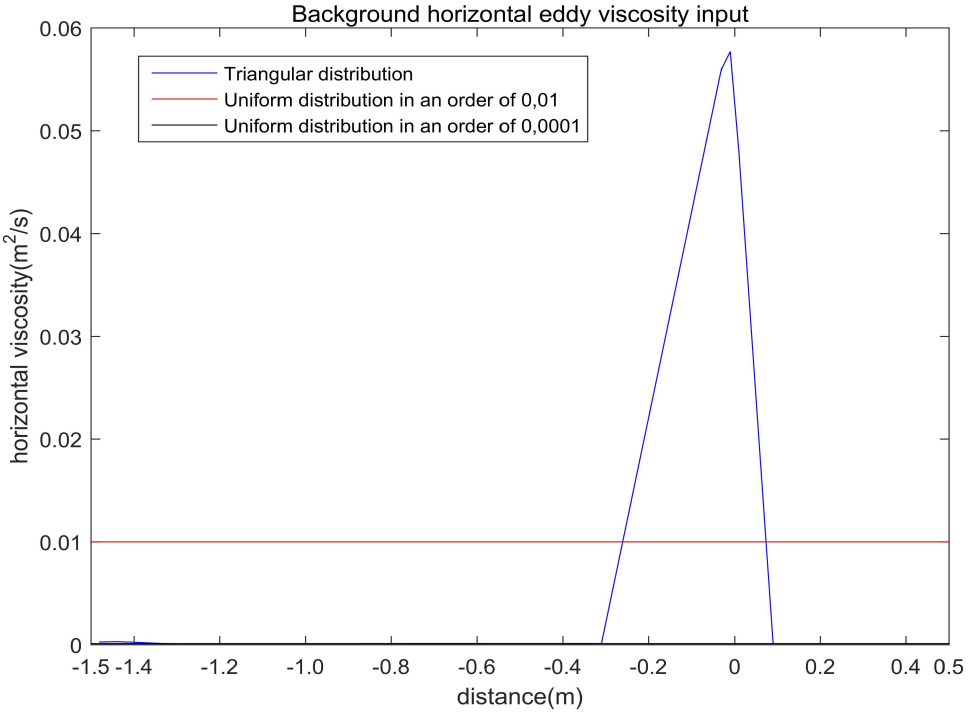

Figure 3.18: Different ways of inputting background horizontal eddy viscosity.

The values of horizontal eddy viscosity of the triangular distribution are calculated from the definition of horizontal Reynolds stress : $-<\overline{u'v'}>=v_t\frac{d\overline{U}}{dy}$. It should be noticed that the triangular distribution is a simplified distribution. The original calculation from flume measurements leads to a smoother distribution. For the sake of simplicity, such a triangular distribution is used but the maximum and minimum values are the same.

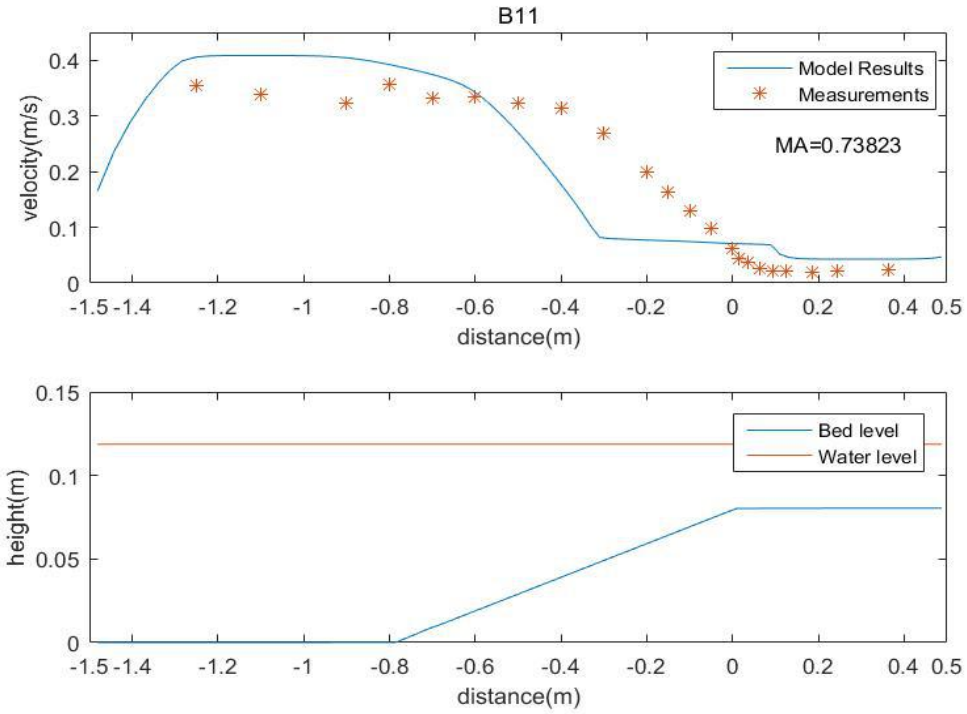

Figure 3.19 : Model results (B11) by inputting triangular distribution of background horizontal eddy viscosity.

As can be seen in Figure 3.19, the depth averaged velocity profile is totally wrong when a triangular distribution of horizontal eddy viscosity is used. The average flow velocity between the region X=-0.3 and X=0.1 is much lower than measurements and it is totally controlled by the value of eddy viscosity. It can be imagined that the model makes the flow in this region very viscous. However, in reality the high eddy viscosity in the shear mixing layer is caused by the presence of eddies. The eddies are generated with a certain period and they also move with the mean flow. Hence, the eddy viscosity should be both time and space varying. Obviously, a space varying background horizontal eddy viscosity in RANS model is not sufficient to model the turbulence. This implies that the model concept of background horizontal eddy viscosity makes it impractical. Therefore, the triangular distribution of eddy viscosity calculated by experimental results should not be used in this study. This leads to tests of inputting different uniform values of background horizontal eddy viscosity.

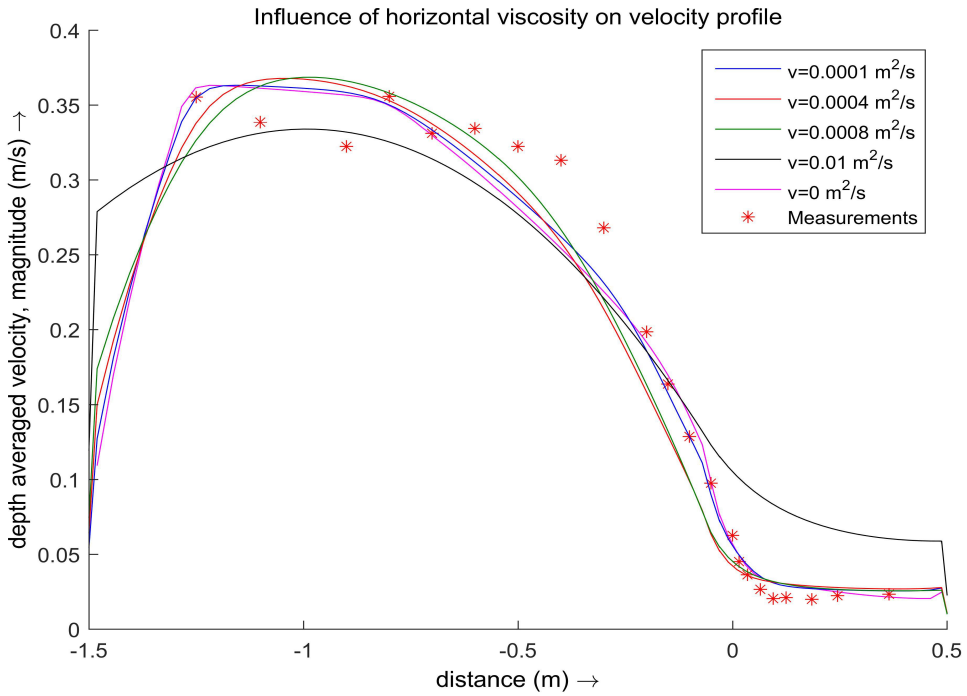

Figure 3.20: Model results by inputting different uniform values of background horizontal eddy viscosity.

Figure 3.20 shows model results by inputting uniform values of background horizontal eddy viscosity with different order of magnitude. When eddy viscosity is zero or in an order of $O(10^{-4})$ [m^2/s], the model results converge and match the measurements quite well. It should be noticed that $\upsilon_H^{back} = 0\ m^2/s$ does not mean total viscosity is zero since in a 2D model the Elder formulation is already built in. In that case $\upsilon^{3D} = \frac{1}{6}\kappa u_* h$ is applied by the model to represent the dispersive effect, which leads to a logarithmic horizontal velocity profile over depth. When eddy viscosity is in an order of $O(10^{-2})$ [m^2/s], the lateral velocity profile generated by the model deviates too much from the measurements. Therefore, an uniform value of background horizontal eddy viscosity with an order of $O(10^{-4})$ [m^2/s] or even smaller should be used in this study. The selection of uniform value of eddy viscosity should be further verified by looking into the eddies generated by these models.

Figure 3.21 shows flow patterns of simulations with different values of υ_H^{back}. Coherent structures become weaker as eddy viscosity increases. When eddy viscosity is as large as 0.0008 m^2/s, eddy is damped out and the flow pattern tends to be regular. In order to observe eddies, $\upsilon_H^{back} \le 0.0004\ m^2/s$ should be applied.

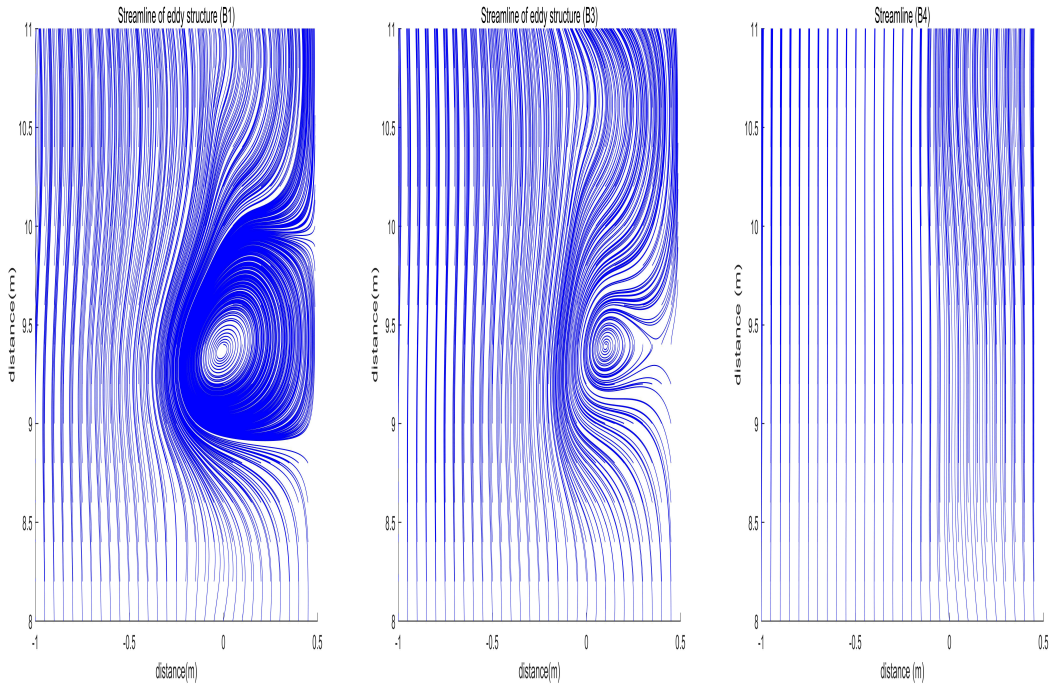

Figure 3.21: Flow patterns of simulations with different background horizontal eddy vicosity. $\upsilon_H^{back} = 0.0001$, 0.0004 and 0.0008 m^2/s from left to right respectively.

After analyzing the lateral velocity profile and flow patterns generated by simulations with different values of υ_H^{back}, it is found that $\upsilon_H^{back} \le 0.0004\ m^2/s$ should be applied. Actually, $\upsilon_H^{back} = 0\ m^2/s$ with only Elder formulation used for the turbulence model is sufficient in this study. However, a very low value of eddy viscosity may leads to instability of the model. In order to make sure the model will not crash in any cases, $\upsilon_H^{back} = 0.0001\ m^2/s$ is used for the reference model in this study.

As discussed previously in this section, an ideal eddy viscosity model should be able to calculate the eddy viscosity, which is both time and space varying. The RANS model in Delft3D-Flow only allows an input of constant value of υ_H^{back} to represent the 2D turbulence, which is not sufficient. In this sense, HLES model should be a better turbulence model. However, as discussed in Section 2.5.3, the large ratio of $H/\Delta x$ suppresses the sub-grid scale eddy viscosity υ_{SGS}, which makes it not necessary to apply HLES model. Therefore, applying the RANS model with $\upsilon_H^{back} = 0.0001\ m^2/s$ is the optimum option in this study.

Also, it is discussed in Section 3.3.2 that the model seems to overestimate the lateral momentum transport in the shear mixing layer. It implies that the RANS model may not be very accurate in calculating the momentum exchange. However, it is still believed that the model is able to capture the changes of flow characteristics when some physical parameters are changed. For example, the eddies are damped out as bed roughness increases or the vegetation patch is removed. Under this assumption, the influence of geometrical settings on penetration of flow is studied in next section.

3.5 Environmental settings and penetration of flow

In mangrove forests, the capability of mangroves to capture sediments leads to accumulation of sediments within the mangrove forests. Hence, the elevation of the floodplain, where the mangroves grow, is usually higher than the main river bed. In Mekong estuarine systems, the slope which connects main river channel and floodplain is around 1/10 (Son, 2017). However, a milder slope was measured in Trang province,Thailand with an angle between 1/1000 to 15/1000 (Horstman,2014). The topography of the mangrove area is influenced by both sediment dynamics and hydrodynamics. The physical processes behind this is still not fully understood. In this study, only the hydrodynamics in a partially vegetated channel is studied due to a lack of data to calibrate the model with sediments.
This section mainly focuses on the influence of slope angle and vegetation desity on the penetration of flow into the forests. Special attention is paid into the horizontal Reynolds stress around vegetation area, which is related to the momentum transport.

3.5.1 Influence of vegetation on penetration of flow

Firstly, the vegetation effects on penetration of flow is studied. Cases of no vegetation, sparse vegetation and dense vegetation are simulated with the same input paramaters as the reference model described in Section 3.3.2. The slope angle is 1/10. Actually, these cases were already conducted in the flume experiments and the results are presented in Secton 3.2.2. The numerical model only works as a tool to analyze the momentum transport around the vegetation edge.

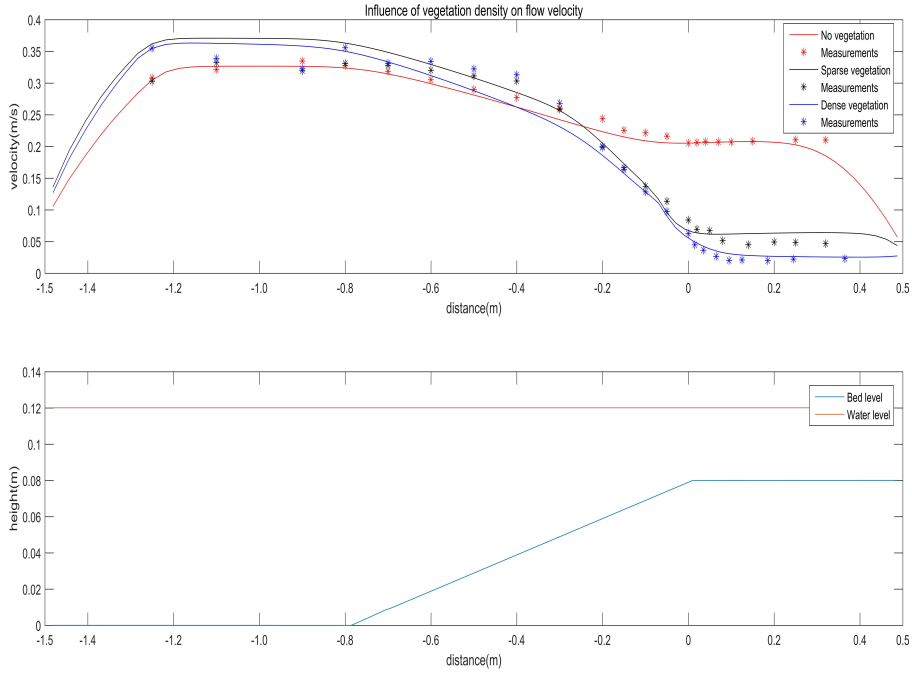

Figure 3.22: A summary of model results and measurements with different vegetation density.

As can be seen in Figure 3.22, after calibration the model is able to estimate the lateral velocity profile quite well when vegetation density changes. Except on the slope, where the velocity is underestimated by the model. The possible reason for this is given in Section 3.3.2. This section, however, mainly focuses on the penetration of flow by looking into the horizontal Reynolds stress calculated from model results. The horizontal Reynolds stress, which is interpreted as momentum transport in this case, is calculated with $T_{xy} \approx \rho_w < \overline{u'v'} >= \rho_w \upsilon_c \frac{\partial U}{\partial y}$. Horizontal eddy viscosity $\upsilon_c = 0.0001 \quad m^2/s$ and it is constant is this case. So the horizontal Reynolds stress only depends on the velocity gradient. Figure 3.23 shows the Influence of vegetation density on horizontal Reynolds stress.

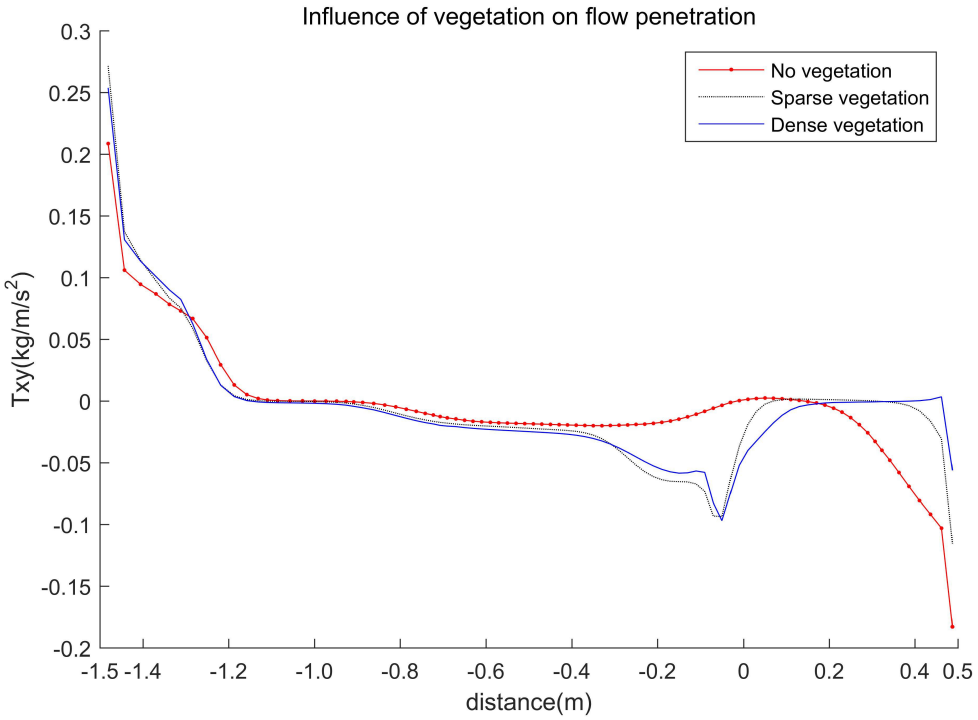

Figure 3.23: Influence of vegetation density on horizontal Reynolds stress with sparse vegetation $(139/m^2)$ and dense vegetation $(550/m^2)$.

As can be seen in Figure 3.23, the presence of vegetation leads to a sharp increase of horizontal Reynolds stress around the vegetation edge. This implies that the vegetation patch strengthen the momentum exchange in the shear mixing layer. It should be noticed that the dense vegetation leads to stronger momentum exchange within the vegetation patch comparing to that of the sparse vegetation. It can even be expected that when sediment is considered, a denser vegetation patch can cause a larger influx of sediment into the mangrove area.

3.5.2 Influence of slope angle on penetration of flow

As described previsouly, the typical slope angle in Mekong estuarine system is 1/10 though gentler slope was measurend in Thailand. This section focuses on the influence of slope angle on penetration of flow. This subject has not been studied in the flume experiments. Although some defect of the model is found previously, it is assumed that the model is able to capture the changes of flow characteristics when physical parameters or environmental settings are changed. Partially vegetated channel with dense vegetation $(550/m^2)$ is simulated with different slope angle but the same model parameters as the reference model. There are two ways of changing geometrical settings. Firstly, only the slope angle is changed so that the wet area also changes. In this way, the cross sectional averaged velocity is changing in different

cases, which makes it less convincing. Secondly, both the slope angle and the width of the main channel is changed so that the wet area does not change. In this way, the cross sectional averaged velocity remain the same. The second method is more convincing theoretically. However, the first method represents the reality better. Because in reality, the erosion can take away the sediment and the wet area can also change. Figure 3.24 shows the results from the first method.

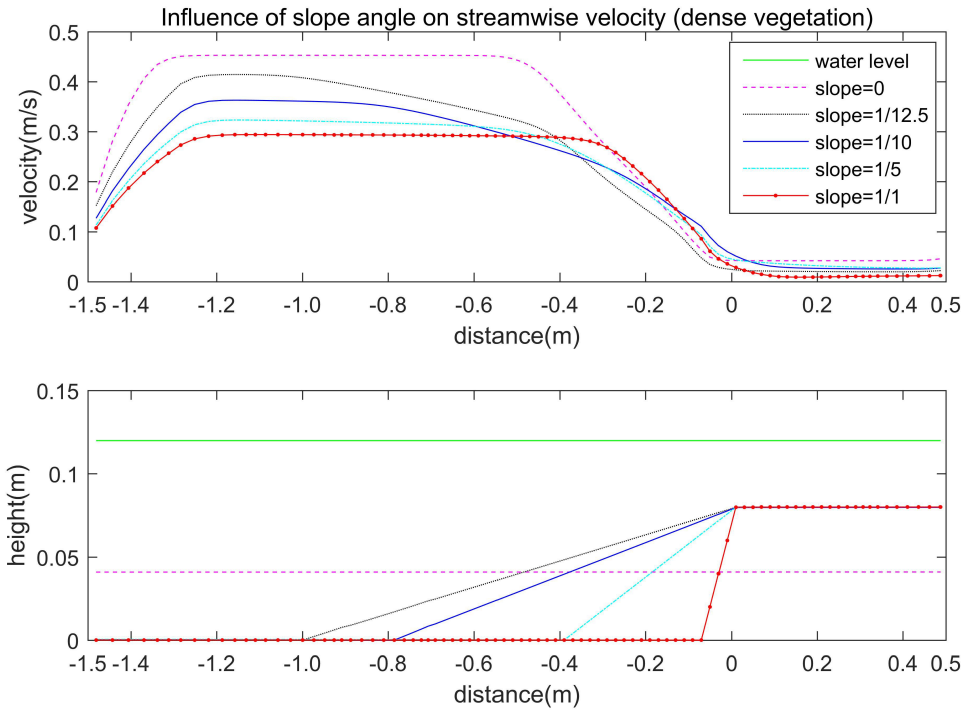

Figure 3.24 : influence of slope angle on lateral profile of streamwise velocity (first method). All the cases are simulated with dense vegetation $(550/m^2)$ between x-coordinate 0 and 0.5 m .

Figure 3.24 summarizes the lateral profile of streamwise velocity in cases with different slope angle. The streamwise velocity magnitude is mainly influenced by the wet area since the upstream discharge is constant. In order to study the effects of slope angle on penetration of flow, a further look into the lateral momentum exchange is needed. Again, the horizontal Reynolds stress, which is interpreted as momentum transport in this case, is calculated with $T_{xy} \approx \rho_w < \overline{u'v'} >= \rho_w \upsilon_c \frac{\partial U}{\partial y}$.

Horizontal eddy viscosity $\upsilon_c = 0.0001 \quad m^2/s$ and it is constant in these cases.

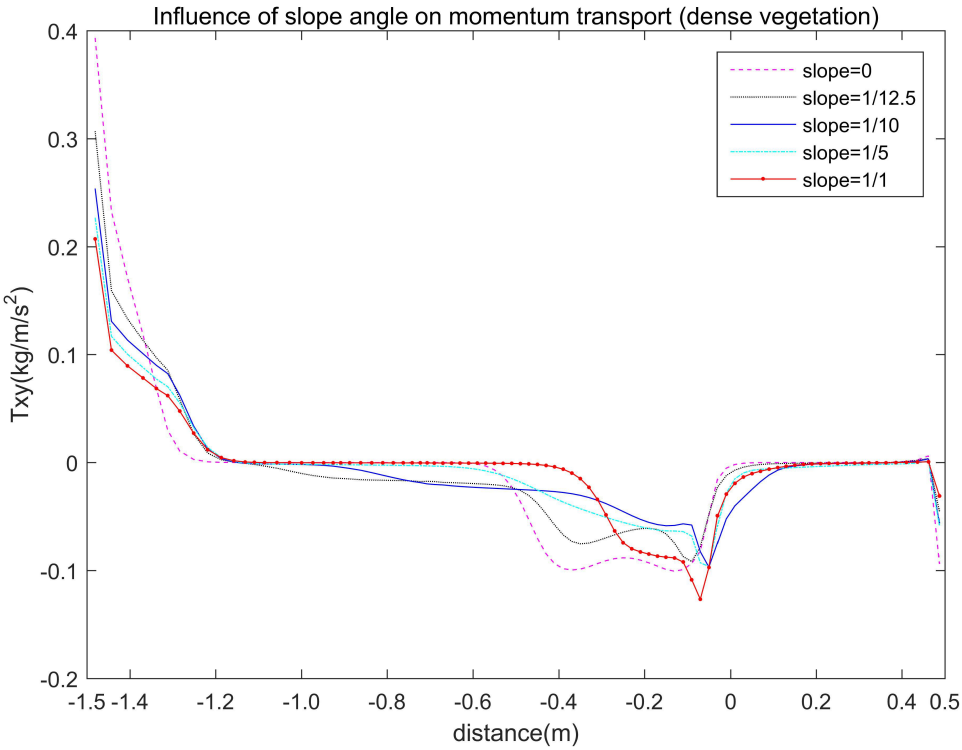

Figure 3.25: Influence of slope angle on horizontal Reynolds stress (first method). Distance=0 m is the edge of vegetation patch.

Figure 3.25 shows the distribution of momentum exchange calculated from model with different slope angle. The horizontal Reynolds stress, which is interpreted as lateral momentum exchange here, is mainly dependent on the lateral velocity gradient. The combined effects of slope angle and vegetation-induced friction dominate the momentum exchange in the shear mixing layer, which makes the situation rather complex. In Figure 3.25, attention should be paid into the area between distance=0 m and distance=0.2 m. It can be seen that with a slope angle of 1/10, the momentum transport into the vegetation patch is larger than that of other slope angle. It implies that a slope angle around 1/10, which is the most typical slope angle in Mekong estuarine system, might be a result of natural selection. Because with a 1/10 slope, the vegetation patch receives most “attack” from the river flow. This conclusion is made under the assumption that the model used in this study is able to estimate the trend of the changes in flow characteristics.

Also, the inner penetration of momentum transport is also reflected in the patterns of coherent structures generated in the shear mixing layer. Figure 3.26 shows the flow patterns of simulations with different slope angle. It can be seen that with a slope angle of 1/10, the strongest eddy structure is observed. This also proves that a slope angle around 1/10 can lead to largest amount of momentum transport into the vegetation patch.

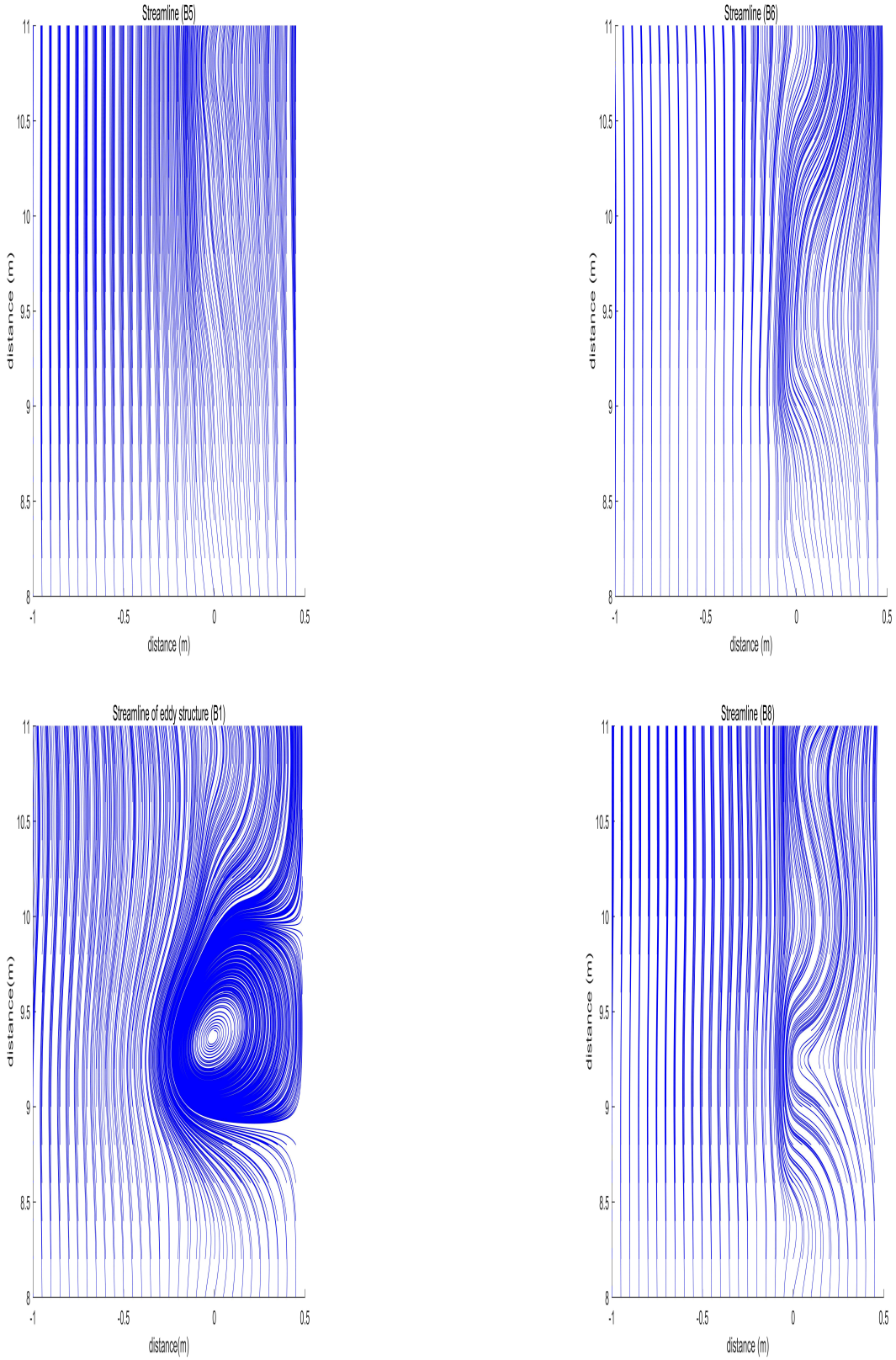

Figure 3.26: flow patterns of simulations with different slope angle. The slope angles of model B5, B6, B1 and B8 are 0, 1/12.5, 1/10 (reference), 1/1 respectively.

In order to make the results more convincing, the second method of chaning geometry is applied so that the cross sectional averaged velocity remains the same in all cases. Figure 3.27 shows the results from the second method.

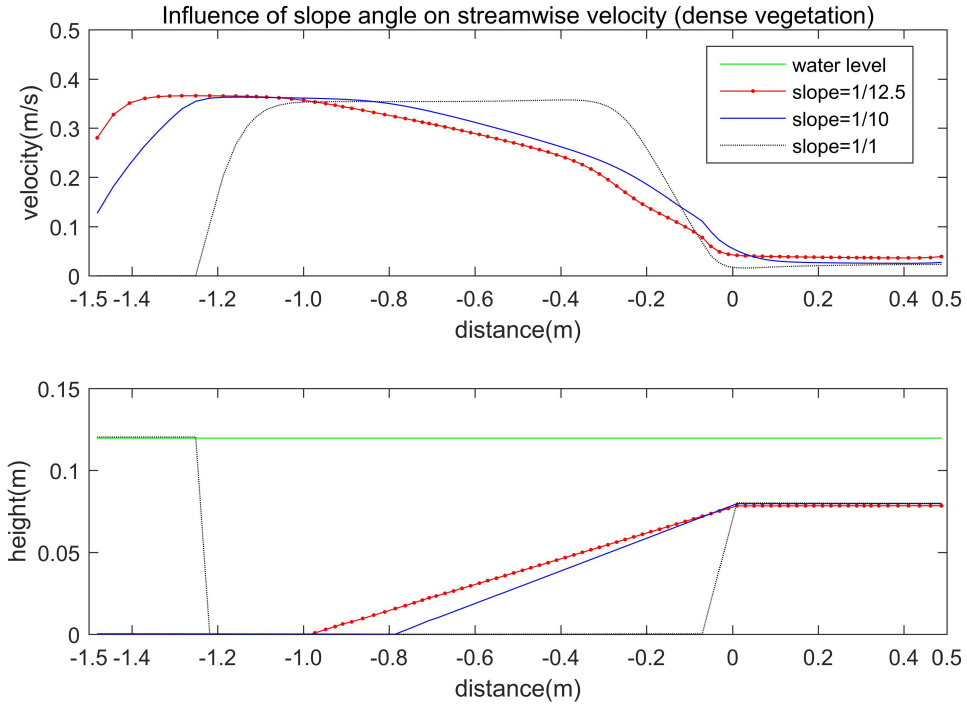

Figure 3.27: Influence of slope angle on lateral profile of streamwise velocity (second method). All the cases are simulated with dense vegetation $(550/m^2)$ between x-coordinate 0 and 0.5 m .

As can be seen in Figure 3.27, the streamwise flow velocity in the main channel remains more or less the same with different slope angle. A further insight into the lateral momentum transport is needed in order to prove the results from the first method. Figure 3.28 shows the distribution of momentum exchange calculated from model with different slope angle (second method).

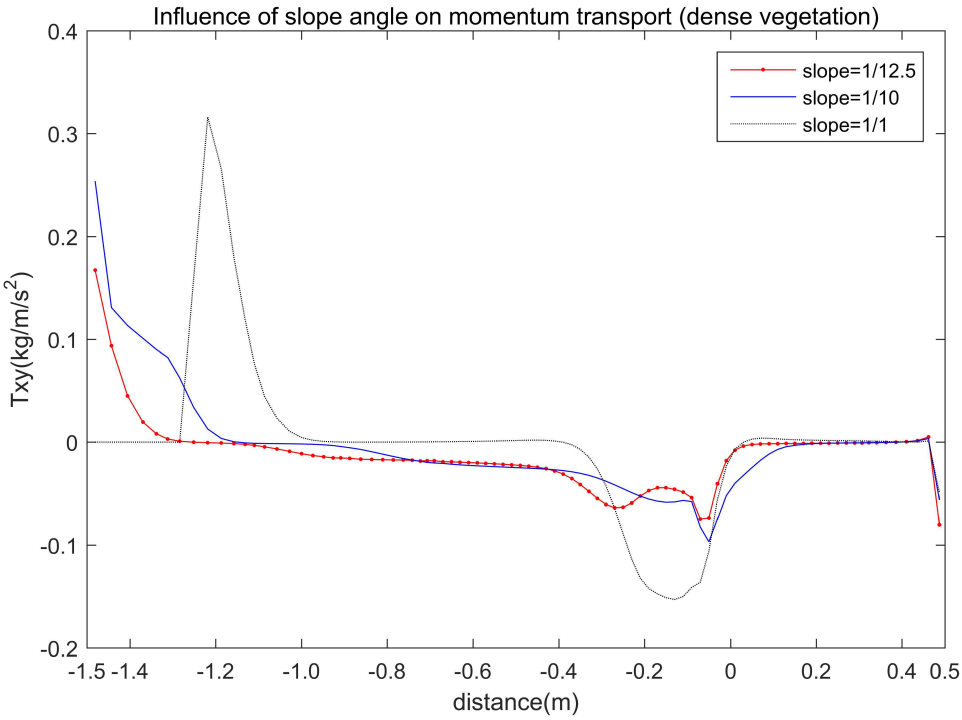

Figure 3.28: Influence of slope angle on horizontal Reynolds stress (second method). Distance=0 m is the edge of vegetation patch.

Comparing with Figure 3.25, it can be seen that a 1/10 slope still leads to largest amount of momentum transport into the vegetation patch. The main difference is that the momentum exchange near the vegetation edge in case of 1/1 slope becomes larger. The possible reason is that a decreasing wet area leads to a larger lateral velocity gradient, which leads to more momentum transport.

4 Synthesis

4.1 Discussion

This section discusses the connection between the small-scale model and large scale model. In order to understand the difference between models with different scales, a large flume scale model is built and tested.

The new model domain is enlarged with a factor of 10 comparing with the flume scale model. The discharge increases with a factor of 100 so that the cross sectional averaged velcoity remains the same. The stem diameter used in the vegetation model also increases with a factor of 10. But the vegetation density is decreased to $5.5/m^2$ in order to keep the volume fraction of obstruction the same as the small scale model. A manning coefficient of 0.015 $m^{1/3}/s$ is applied, which is a typical value for large scale simulations. The background eddy viscosity is the most important parameters in this test. A value of 0.0001 m^2/s is used, which is the same as the small flume-scale model. It should be noticed that the reflection parameter alpha is set to 20 at the water level boundary in order to make the model numerically stable. This value can be estimated with Equation 3.1. Figure 4.1 and Figure 4.2 show the model results.

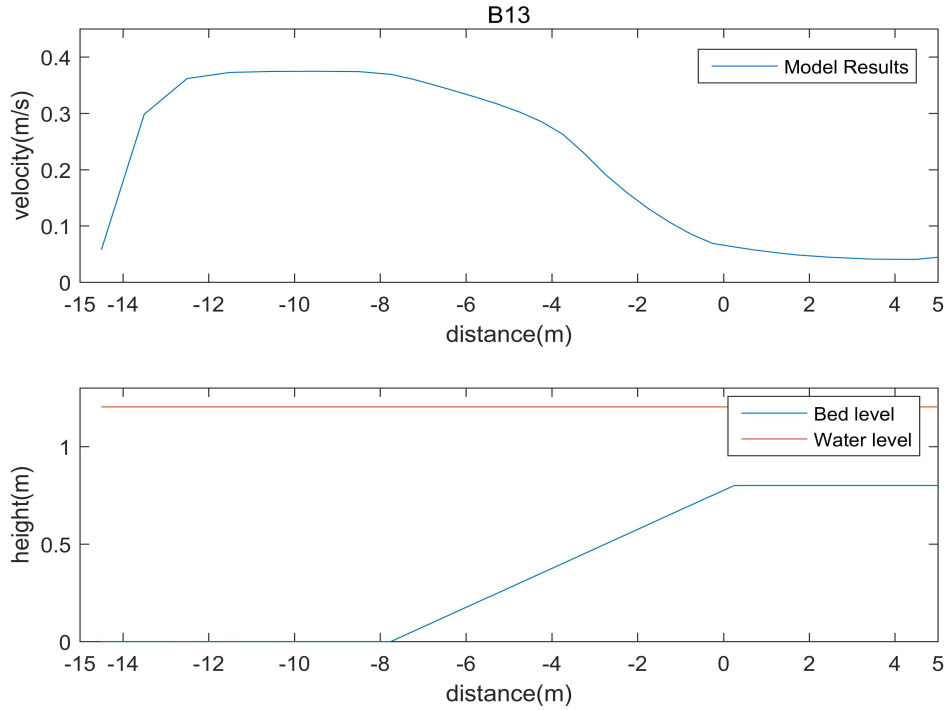

Figure 4.1: Lateral velocity profile from large-scale model. The velocity profile is captured at 100 meters away from the upstream boundary.

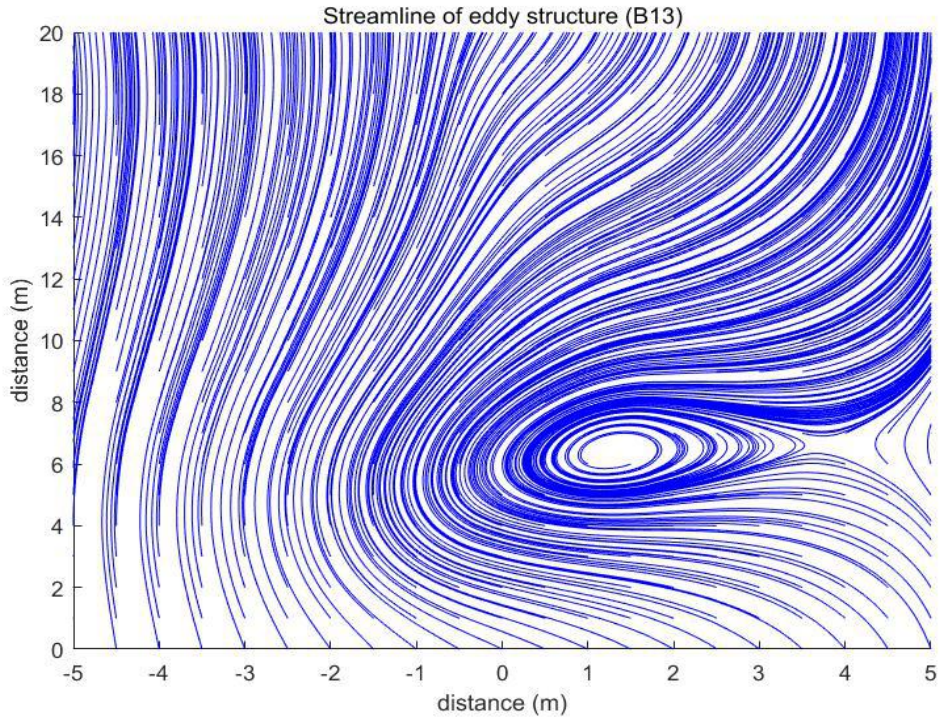

Figure 4.2: Eddy structure captured in the large scale model. The area between X-coordinate “0” and “5” meters is the vegetation area.

As can be seen in Figure 4.1, after the model domain is enlarged with a factor of 10, the velocity profile stays more or less the same comparing the small scale model (Figure 3.12). This is because these two models have the same cross sectional averaged velocity. Figure 4.2 shows the eddy structure captured around the vegetation edge. The eddy structure almost fully penetrates into the floodplain. Although it is not possible to calibrate this large scale model with measurements, it can be concluded that the model is able to produce reasonable results with such a model setup.

In order to gain more insight into the connection between small scale model and large scale model, a comparison is drawn. Table 4.1 summarizes the important information of flume experiemnts, flume-scale model and prototype model. Although the large flume-scale model and prototype model have not been calibrated, the input parameters are listed below so that the model can work properly.

Table 4.1: Comparison of parameters between flume, flume-scale model and prototype model.

	Flume	**Small flume-scale model**	**Large flume-scale model**	**Prototype model**
Domain	3x20 m	3x20 m	30x200 m	1100x2000 m
Relative depth (Dr)	0.04 m/0.12 m	0.04 m/0.12 m	0.4m /1.2 m	0.5 m/7.5 m
Slope angle	1/10	1/10	1/10	1/10
Re (floodplain)	900-7500	900-7500	$O(10^4)$	$O(10^4)$
Bed roughness (Manning)	$O(10^{-3})$	0.0021	0.015	$O(10^{-1})$
Drag coefficient		0.8	0.8	1
Horizontal eddy viscosity (input value)		0.0001	0.0001	
Horizontal eddy viscosity (maximum output value)	0.06	0.0012	0.0027	
Vegetation input	Real cylinders	Vegetation model	Vegetation model	Vegetation model

As can be seen in Table 4.1, the flume is designed so that the Reynolds number in the flume can be closer to the prototype. Same slope angle is adopted in flume and prototype. The relative depth in the flume is also designed to reproduce the relative depth in prototype, although there is still some difference. This is due to the restriction of the flume facility. The input parameters are compared to obtain a better understanding of model with different scale.

Firstly, the bed roughness in the small flume-scale model is much smaller than the large scale model. This implies that the bed roughness input should be smaller in a small scale flow than that in a large-scale flow. Secondly, the drag coefficient in both models are around 1. This means the drag coefficient should not deviate too much from 1. Thirdly, it seems that a background eddy viscosity with a value of 0.0001 m^2/s is also applicable in large scale flow. However, the values of horizontal eddy viscosity calculated from flume and model output are quite different. There might be three reasons for this: 1. The horizontal eddy viscosity is a calibration parameter and it varies in flow with different scales; 2. The horizontal eddy viscosity is largely influenced by the vegetation. The vegetation model in Delft3D only represents the overall effect of vegetation drag force and it is not sufficient. 3. The RANS model in Delft3D does not simulate the momentum transport accurately.

4.2 Conclusion

The research questions are summarized as follows:

1. How do bed roughness, drag coefficient and horizontal eddy viscosity influence the flow characteristics in a partially vegetated channel?

2. How do geometrical settings (bank flow with different slope angle and channel flow) influence the momentum transport at the flow-vegetation interface ?

In order to answer the research questions through model results, calibration of the numerical model is required to determine the model parameters. In this study, the most influential parameters include bed roughness, drag coefficient and background horizontal eddy viscosity. Bed roughness and drag coefficient are physical parameters and they should be within a reasonable range of value. Combining the flume measurements and calibration of the model **suggests a manning coefficient of 0.0021** $m^{1/3}/s$ **.** This value is around an order of magnitude smaller than the bed roughness in a large scale flow (prototype). **This implies that the bed roughness input should be smaller in a small scale flow than that in a large-scale flow.** The drag coefficient is 1 for single cylinders and **in this study a value of 0.8 is recommended after calibration of the model.** The horizontal eddy viscosity is more of a calibration parameter than a physical parameter and it varies a lot in different types of flow. **An uniform horizontal eddy viscosity value of** $10^{-4}\ m^2/s$ **is suggested according to calibration of the model. In large scale flow, it seems that a background eddy viscosity value of** $10^{-4}\ m^2/s$ **is also applicable. It is recommended to keep this value as small as possible.**

Bed roughness is the dominant factor in the case without vegetation. An increasing manning coefficient (rougher bed) leads to a decrease of flow velocity in both main channel and floodplain. **In the case of model with vegetation, the effects of bed roughness is overwhelmed by drag coefficient. However, a rougher bed dampens the energy in the flow and therefore weakens the eddies.**

Drag coefficient represents the vegetation-induced friction. **A higher drag coefficient leads to a lower flow velocity at floodplain and a higher flow velocity in the main channel.** When the drag coefficient increases, more water flow is deflected into the main channel, which leads to a higher flow velocity in the main channel.

The flow characteristics within the shear mixing layer are dominated by the horizontal eddy viscosity. With an uniform value of background horizontal eddy viscosity in an order of $O(10^{-4})$ [m^2/s] or even smaller, the model generates best estimation of lateral velocity profile. **Coherent structures become weaker as**

background eddy viscosity increases. When eddy viscosity is as large as 0.0008 m^2/s , eddy is damped out and the flow pattern tends to be regular. In order to observe eddies, $\upsilon_H^{back} \leq 0.0004 \ m^2/s$ should be applied. In large scale flow the background horizontal eddy viscosity might be larger considering the stability of the model. However the background horizontal eddy viscosity should not be too large since the coherent structures are damped out as background eddy viscosity increases.

Some limitation of the RANS model in Delft3D-Flow has been found. **Firstly, a space varying background horizontal eddy viscosity (e.g. Triangular distribution) in RANS model is not sufficient to model the turbulence since in reality the horizontal eddy viscosity should be both time and space varying.** This implies that the model concept of background horizontal eddy viscosity is not very practical. **Secondly, after analyzing the model results, it is found that the model is not very accurate in predicting the momentum transport in the shear mixing layer and the momentum exchange is too much around the edge of vegetation patch.** This leads to an underestimation of flow velocity in the shear mixing layer and an overestimation of eddy penetration into the vegetation patch. **The possible reason is that the vegetation model only takes into account the overall effects of vegetative drag force instead of considering the effects of each single stem.**

Under the assumption that the model is able to capture the changes of flow characteristics when physical parameters or environmental settings are changed, a further research focuses on the influence of environmental settings on flow characteristics. Regarding the vegetation density, the presence of vegetation leads to a sharp increase of horizontal Reynolds stress around the vegetation edge. **This implies that the vegetation patch strengthen the momentum exchange in the shear mixing layer.** Also, a denser vegetation patch leads to stronger momentum exchange within the vegetation patch.

The slope angle is also influential in case with dense vegetation on the floodplain. **A slope angle around 1/10, which is the most typical slope angle in Mekong estuarine system, leads to the largest amount of momentum transport into the vegetation patch.** Also, with a slope angle of 1/10 the strongest eddy structure is observed.

Regarding the predictive ability of the model, **it is believed that the model can give reasonable results for lateral velocity profile and large scale turbulence.** It is still applicable to cases when the requirement of accuracy is not very high (e.g. studying the influence of vegetation on flow characteristics).

4.3 Recommendations

After this study, some limitation of RANS model in Delft3D-Flow has been found. As described in section 3.3.2, the model overestimates the momentum transport at the edge of vegetation patch. The possible reason is that the vegetation model only takes into account the overall effects of vegetative drag force instead of considering the effects of each stem. Hence, the stem-scale turbulence is left out by the vegetation model. **It is recommended to improve the vegetation model by considering the effects of each single stem and distribution of the vegetation.**

Section 3.4.3 describes different ways of inputting background horizontal eddy viscosity. It is found that inputting a space varying eddy viscosity is not practical since in reality the eddy viscosity is both time and space varying. **It is recommended to design and apply a turbulence closure model in RANS model, which is able to calculate the values of eddy viscosity over time and space. If this is not possible, then a 3D LES model is recommended since it is especially designed for simulations of turbulent flow. Also, background eddy viscosity is not needed as an input, which makes it easier to calibrate.**

In this study, only the flume-scale model is calibrated. However, the connection between flume-scale model and prototype-scale model is not well understood. **It is recommended to calibrate the prototype scale model with field measurements and explore the relationship between flume-scale model and prototype-scale model.**

References

Alongi, D.M. (2002). Present state and future of the world's mangrove forests. Environmental Conservation, 29(3), 331-349.

Aucan, J. & P.V. Ridd (2000). Tidal asymmetry in creeks surrounded by saltflats and mangroves with small swamp slopes. *Wetlands Ecology and Management*, 8(4), 223-232.

Buckman, L.J (2013). Hydrodynamics of partially vegetated channels: Stem drag forces and application to an in-stream wetland concept for tropical, urban drainage systems, 7-14. uuid:71f7e38d-a05b-4e6e-bb84-88fa4d6f31b9.

Cintron, G. & Y. Schaeffer-Novelli (1984). Methods for studying mangrove structure. In: S.C. Snedaker (Ed.), The mangrove ecosystem: research methods. *Monographs on Oceanographic Methodology*. UNESCO, Paris, 91-113.

Danielsen, F., M.K. Sørensen, M.F. Olwig, V. Selvam, F. Parish, N.D. Burgess, T. Hiraishi, V.M. Karunagaran, M.S. Rasmussen, L.B. Hansen, A. Quarto & N. Suryadiputra (2005). The Asian Tsunami: A protective role for coastal vegetation. *Science*, 310(5748), 643.

Deltares (2016). Delft3D-Flow Manual. The Netherlands.

Doody, J., 2004. ‘Coastal squeeze’ -an historical perspective. *Journal of Coastal Conservation*, 737 10(1), 129-138.

Duke, N.C. (1992). Mangrove floristics and biogeography. In: A.I. Robertson and D.M. Alongi (Eds.), Tropical mangrove ecosystems. *American Geophysical Union*, Washington DC, 63-100.

Duke, N.C., J.-O. Meynecke, S. Dittmann, A.M. Ellison, K. Anger, U. Berger, S. Cannicci, K. Diele, K.C. Ewel, C.D. Field, N. Koedam, S.Y. Lee, C. Marchand, I. Nordhaus & F. Dahdouh-Guebas (2007). A world without mangroves? *Science*, 317(5834), 41-42.

Ewel, K.C., J.A. Bourgeois, T.G. Cole & S. Zheng (1998). Variation in environmental characteristics and vegetation in high-rainfall mangrove forests, Kosrae, Micronesia. *Global Ecology and Biogeography Letters*, 7(1), 49-56.

Giri, C., E. Ochieng, L.L. Tieszen, Z. Zhu, A. Singh, T. Loveland, J. Masek & N. Duke (2011). Status and distribution of mangrove forests of the world using earth observation satellite data. *Global Ecology and Biogeography*, 20(1), 154-159.

Hirt, C.W.- Phys. Fluids. Suppl. II, 219-227 (1969).

Horstman, Erik Martijn (2014). The mangrove tangle: short-term bio-physical interactions in coastal mangroves. Thesis.

Hu, K., P. Ding, Z. Wang & S. Yang (2009). A 2D/3D hydrodynamic and sediment transport model for the Yangtze Estuary, China. *Journal of Marine Systems*, 77(1–2), 114-136.

Kobashi, D. & Y. Mazda (2005). Tidal flow in riverine-type mangroves. *Wetlands Ecology and Management*, 13(6), 615-619.

Lugo, A.E. & S.C. Snedaker (1974). The ecology of mangroves. *Annual Review of Ecology and Systematics*, 5, 39-64.

Mazda, Y., E. Wolanski & P.V. Ridd (2007). The role of physical processes in mangrove environments: manual for the preservation and utilization of mangrove ecosystems. Terrapub, Tokyo.

Nash, J.E. & J.V. Sutcliffe (1970). River flow forecasting through conceptual models part I — A discussion of principles. *Journal of Hydrology*, 10(3), 282-290.

Nepf, Heidi (2012), Hydrodynamics of vegetated channels, *Journal of Hydraulic Research*, 50 (3), 262–279.

Nepf, H. M. (2012). Flow and Transport in Regions with Aquatic Vegetation. *Annual Review of Fluid Mechanics*,44(1),123-142. doi:10.1146/annurev-fluid-120710-101048

Nepf, H. M. (2012). Hydrodynamics of vegetated channels. *Journal of Hydraulic Research*, 50(3), 262-279. doi:10.1080/00221686.2012.696559

Phan, N.H. and Hoang, T.S., 1993. Mangrove of Vietnam. Bangkok: IUCN, 173p.

Schiereck, Gerrit J. (2012). Introduction to Bed, Bank and Shore Protection. 2nd ed. Delft: VSSD, 24-28.

Siniscalchi, F., Nikora, V. I., and Aberle, J. (2012), Plant patch hydrodynamics in streams: Mean flow, turbulence and drag forces, Water Resources Research, 48, W01,513.

Temmerman, S., T.J. Bouma, G. Govers & D. Lauwaet (2005a). Flow paths of water and sediment in a tidal marsh: Relations with marsh developmental stage and tidal inundation height. *Estuaries*, 28(3), 338-352.

Temmerman, S., T.J. Bouma, J. Van de Koppel, D.D. Van der Wal, M.B. De Vries & P.M.J. Herman (2007). Vegetation causes channel erosion in a tidal landscape. *Geology*, 35(7), 631-634.

Tomlinson, P.B. (1986). The botany of mangroves. *Cambridge tropical biology series*. Cambridge University Press, Cambridge, UK.

Uittenbogaard, R. E., 1998. Model for eddy diffusivity and viscosity related to sub-grid velocity and bed topography. *Tech. rep., WL | Delft Hydraulics*, Delft, The Netherlands.

Uittenbogaard, R. E., dec. 2000. Hydrodynamics of flow over plants, internal communication. *Tech. rep., WL | Delft Hydraulics*, Delft, The Netherlands.

Uittenbogaard, R.E., van Vossen, B., 2004. Subgrid-scale model for quasi-2D turbulence in shallow water. In: Jirka, Uijttewaal (Eds.), Shallow Flows.

Uittenbogaard, R. E. and B. Van Vossen, 2003. "Subgrid-scale model for Quasi-2D turbulence in shallow water." In: *Shallow flows: proceedings of the international symposium*, pages 575-582.

Vossen, B. van, 2000. Horizontal Large Eddy simulations; evaluation of flow computations with Delft3D-FLOW. *Tech. Rep. MEAH-197, WL | Delft Hydraulics*, Delft, The Netherlands, 23-40.

White, Brian, and Nepf, Heidi (2008), A vortex-based model of velocity and shear stress in a partially vegetated shallow channel, *Water Resources Research*, 44, W01,412.

Woodroffe, C.D. (1992). Mangrove sediments and geomorphology. In: A.I. Robertson and D.M. Alongi (Eds.), Tropical mangrove ecosystems. *American Geophysical Union*, Washington DC, 7-41.

Zong, Lijun, and Nepf, Heidi (2010), Flow and deposition in and around a finite patch of vegetation, *Geomorphology*, 116, 363–372.

Appendix A

Experimental results

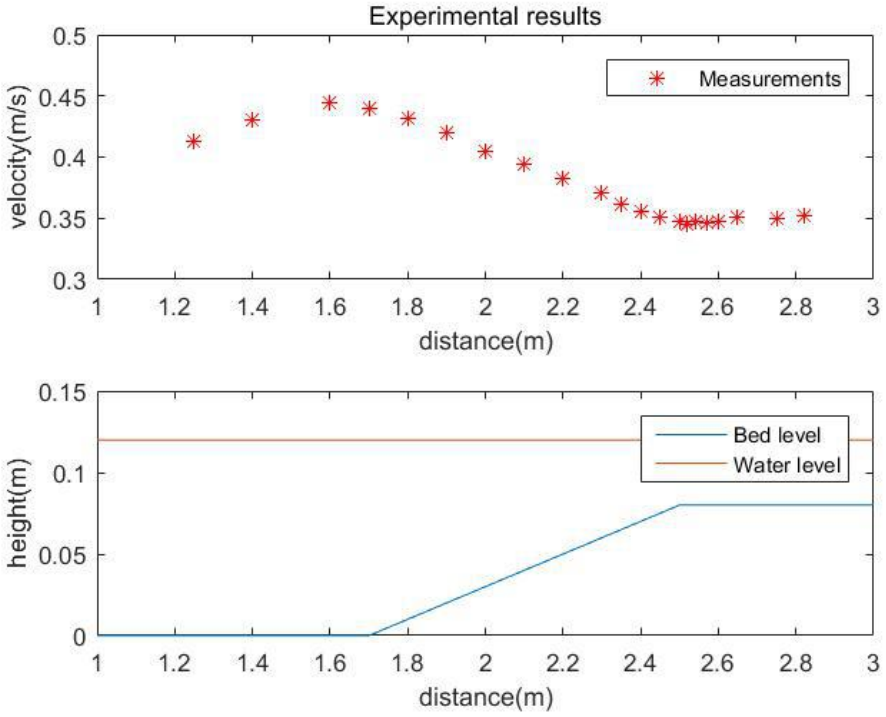

Figure A.1: Experimental results of 80 l/s discharge, 14 cm water level, 0.5 m floodplain width without cylinders. The velocity is measured at 4.8 meters from the beginning of cylinders.

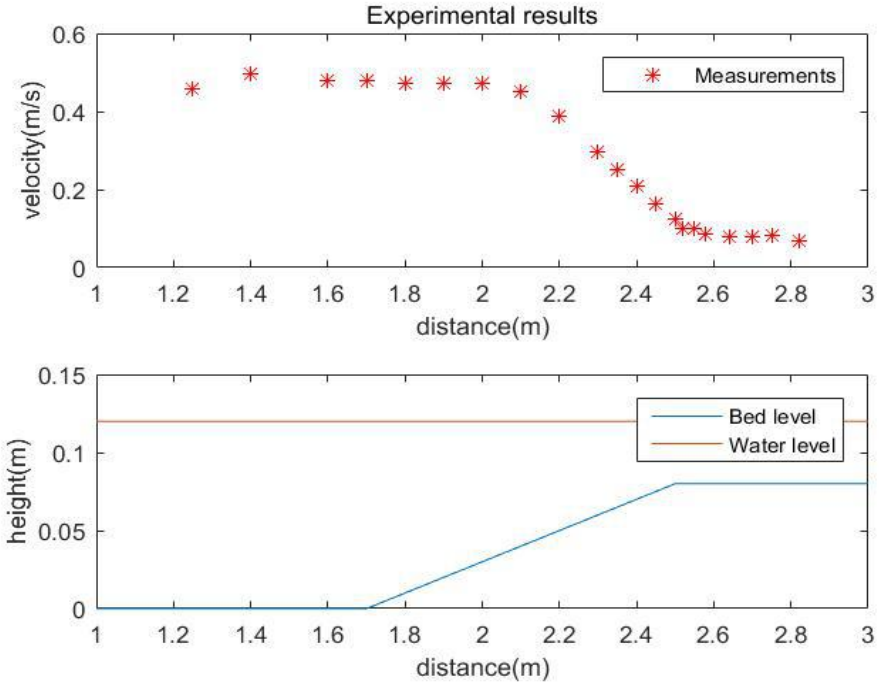

Figure A.2: Experimental results of 80 l/s discharge, 14 cm water level, 0.5 m floodplain width with sparse cylinders (139 cylinders/ m^2). The velocity is measured at 4.8 meters from the beginning of cylinders.

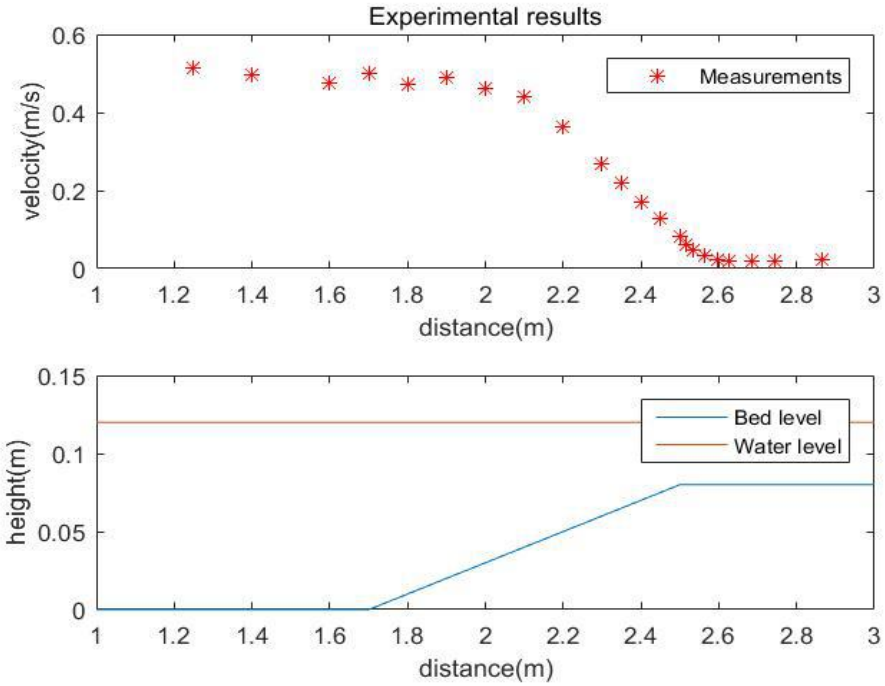

Figure A.3: Experimental results of 80 l/s discharge, 14 cm water level, 0.5 m floodplain width with dense cylinders (550 cylinders/ m^2). The velocity is measured at 4.8 meters from the beginning of cylinders.

Appendix B

Summary of model set up

	Horizontal eddy viscosity m^2/s	Bed roughness (manning) $m^{1/3}/s$	Cd	HLES	vegetation density	Mangrove width	Time step (minutes)	Vertical layerness	Others
A1	0.0001	0.0021 Partial(0.002)	0	No	0	0	0.0001	1	Q=45 l/s, Alpha=2, W=12 cm, Slope=1/10
A2	0.0001	0.0084 Partial(0.002)	0	No	0	0	0.0001	1	Q=45 l/s, Alpha=2, W=12 cm, Slope=1/10
A3	0.0001	0.0021 Partial(0.002)	0	No	0	0	0.0001	1	Q=45 l/s, Alpha=2, W=12 cm, Slope=1/1
A4	0.0001	0.0021 Partial(0.002)	0	No	0	0	0.0001	1	Q=45 l/s, Alpha=2, W=12 cm, Slope=1/12.5
B1	0.0001	0.0021 Partial(0.002)	0.8	No	550	0.5	0.0001	1	Q=45 l/s, Alpha=2, W=12 cm, Slope=1/10
B2	0.0001	0.0021 Partial(0.002)	1.5	No	550	0.5	0.0001	1	Q=45 l/s, Alpha=2, W=12 cm, Slope=1/10
B3	0.0004	0.0021 Partial(0.002)	0.8	No	550	0.5	0.0001	1	Q=45 l/s, Alpha=2, W=12 cm, Slope=1/10

B4	0.0008	0.0021 Partial(0.002)	0.8	No	550	0.5	0.0001	1	Q=45 l/s, Alpha=2, W=12 cm, Slope=1/10
B5	0.0001	0.0021 Partial(0.002)	0.8	No	550	0.5	0.0001	1	Q=45 l/s, Alpha=2, W=12 cm, Slope=0
B6	0.0001	0.0021 Partial(0.002)	0.8	No	550	0.5	0.0001	1	Q=45 l/s, Alpha=2, W=12 cm, Slope=1/12.5
B7	0.0001	0.0021 Partial(0.002)	0.8	No	550	0.5	0.0001	1	Q=45 l/s, Alpha=2, W=12 cm, Slope=1/5
B8	0.0001	0.0021 Partial(0.002)	0.8	No	550	0.5	0.0001	1	Q=45 l/s, Alpha=2, W=12 cm, Slope=1/1
B9	0.0001	0.0084 Partial(0.002)	0.8	No	550	0.5	0.0001	1	Q=45 l/s, Alpha=2, W=12 cm, Slope=1/10
B10	0.0001	0.0021 Partial(0.002)	1.0	No	550	0.5	0.0001	1	Q=45 l/s, Alpha=2, W=12 cm, Slope=1/10
B11	Triangular distribution	0.0021 Partial(0.002)	0.8	No	550	0.5	0.00005	1	Q=45 l/s, Alpha=2, W=12 cm, Slope=1/10
B12	0.0001	0.0021 Partial(0.002)	0.8	No	139	0.5	0.0001	1	Q=45 l/s, Alpha=2, W=12 cm, Slope=1/10
B13	0.0001	0.0021 Partial(0.002)	0.8	No	5.5	0.5	0.0001	1	30x200m domain Q=4500 l/s, Alpha=20, W=120 cm, Slope=1/10